Meteoritics & Planetary Science 39, Nr 3, 367–386 (2004)
Abstract available online at http://meteoritics.org

Simulation of the interaction of galactic cosmic ray protons with meteoroids: On the production of ^{3}H and light noble gas isotopes in isotropically irradiated thick gabbro and iron targets

I. LEYA,[1,2*] F. BEGEMANN,[3] H. W. WEBER,[3] R. WIELER,[2] and R. MICHEL[1]

[1]Center for Radiation Protection and Radioecology, University of Hannover, Hannover, Germany
[2]Isotope Geochemistry and Mineral Resources, NO C61, Zürich, Switzerland
[3]Max-Planck-Institut für Chemie (Otto-Hahn-Institut), Mainz, Germany
*Corresponding author. E-mail: Leya@erdw.ethz.ch

(Received 12 June 2003; revision accepted 15 January 2004)

Abstract–Thick spherical targets, one made of gabbro (R = 25 cm) and one made of iron (R = 10 cm), were irradiated isotropically with 1.6 GeV protons at Laboratoire National Saturne (LNS)/Saclay to simulate the interactions of galactic cosmic ray protons with meteoroids in space. At various depths, both artificial meteoroids contained a large number of high-purity, single-element target foils and chemical compounds of up to 28 target elements. In these individual target foils, the elemental production rates of radionuclides and noble gas isotopes were measured. Here, we report the results for the light noble gas isotopes ^{3,4}He, ^{20,21,22}Ne, and ^{36,38,39}Ar for the most cosmochemically relevant target elements as well as for some meteoritic material from Jilin, Farmington, and Cape York. From ^{3}He analyses done several years apart, ^{3}H diffusive losses during sample storage have been obtained, and direct as well as cumulative ^{3}He production rates for O, Mg, Al, Si, Fe, Ni, and the meteoritic material are given. Losses by diffusion of tritium from metallic Mg and Fe are found to occur on time scales of months, while metallic Al, Si, and stone meteorites are much more retentive. The production rate ratios $P(^{3}H)/P(^{3}He)_d$ obtained in the simulation experiments are 0.73, 1.28, and 1.16 for O, Al, and Si, respectively. These rates are based on our best knowledge about the ^{3}H and ^{3}He production rates and should, therefore, replace data published earlier (Leya et al. 2000a). The earlier calculations for ^{4}He, ^{20,21,22}Ne, and ^{36,38,39}Ar remain valid.

The new modeled correlation $^{3}He_{cum}/^{21}Ne$ versus $^{22}Ne/^{21}Ne$ for chondrites exposed to cosmic rays with an energy spectrum characterized by a modulation parameter of Φ = 650 MeV is in fair agreement with the empirical relationship ("Berne plot"). However, for small meteorites and little shielding in larger ones, there are systematic differences that most likely are due to an underestimation of the spallogenic $^{22}Ne/^{21}Ne$ ratio by ~2%.

INTRODUCTION

In years past, five second-generation, thick-target experiments have been performed to study the interactions of galactic cosmic ray protons with extraterrestrial matter in space. In all previous "classical," thick-target irradiations, the targets were always at rest, being irradiated in 2π geometry, and model calculations were necessary to convert the measured lateral and vertical distributions of reaction products to the case of an isotropic irradiation as it applies to meteoroids in space. However, it has been shown that a simple but ingenious combination of lateral and rotational movements of the targets during irradiation perfectly simulates an isotropic irradiation (Michel et al. 1986, 1989). In such second-generation experiments, artificial stony and iron meteoroids with radii between 5 cm and 25 cm were irradiated isotropically with 600 MeV or 1.6 GeV protons, respectively, to simulate the build-up of secondary particle cascades. A large number of single-element targets, chemical compounds, and degassed meteoritic materials were placed inside the spheres at various positions. Here, we present the results for the production of tritium and the light noble gases from cosmochemically relevant elements and some meteoritic material irradiated with 1.6 GeV protons within a gabbro sphere (R = 25 cm) and an iron sphere (R = 10 cm). Both experiments were performed at the Laboratoire National Saturne (LNS)/Saclay.

The elemental production rates obtained from the five irradiation experiments provide the basis for an evaluation of calculations based on a purely physical model for the production rates (e.g., Michel et al. 1991, 1996; Leya 1997; Leya et al. 2000a, b). Briefly, the model is based on primary and secondary particle spectra, calculated with Monte-Carlo methods, and the excitation functions of the relevant nuclear reactions. For proton-induced reactions, the database is fairly complete, but for neutron-induced reactions, cross section data are still very scarce. To overcome this problem, we derived the neutron excitation functions by subtracting from the total (i.e., proton- plus neutron-induced) production rates, determined in all five simulation experiments, the calculated proton-induced component (see Leya 1997; Leya and Michel 1997; Leya et al. 2000b). From these data, the neutron excitation functions were then calculated by an energy-dependent, least-squares adjustment procedure. The resulting production rates for ^{4}He, $^{20, 21, 22}Ne$, and $^{36, 38, 39}Ar$ in stony meteoroids, and for 2π exposure geometries, have already been published in Leya et al. (2000a, 2001).

We also present data on the ^{3}He and ^{3}H production rates as well as on ^{3}H diffusive losses from the targets during sample storage. To evaluate these losses, aliquots of metallic Mg, Al, Si, and Fe targets from the two 1.6 GeV simulations and from a 600 MeV experiment performed earlier (Michel et al. 1989) were analyzed several years apart. In addition, some samples were encapsulated in glass ampoules about 300 days after irradiation and stored for about 10 years, which allows us to quantify ^{3}H diffusive losses during sample storage. The modeled cumulative $^{3}He_{cum}$ production rates are combined with the production rates of ^{21}Ne and ^{22}Ne (cumulative), and the ensuing $^{3}He_{cum}/^{21}Ne$ versus $^{22}Ne/^{21}Ne$ correlation is compared with the empirical "Berne plot" (Eberhardt et al. 1966; Nishiizumi et al. 1980).

EXPERIMENTAL PROCEDURES

The Artificial Meteoroids

The two artificial meteoroids with radii of 25 cm and 10 cm were made of gabbro and iron, respectively. The chemical compositions are given in Table 1. More than 1400 and 850 individual targets were placed inside the gabbro and iron spheres, respectively (Leya et al. 2000b), comprising up to 28 different elements ranging in mass from C to Au. In the case of O, Na, S, K, and Ca, single-element targets were deemed impractical. The compounds chosen instead (meteoritic FeS [troilite], commercial FeS_2, Na_2WoO_4, Na_2MoO_4, K_2MoO_4, and $CaMoO_4$) were such that contamination of the noble gas mass spectrometers by unwanted molecular species was avoided (no halogens!), and moreover, the contributions to the production of Ne and Ar from other constituents of the compounds were either zero or at least very small.

We present the results for the light noble gases from O, Na, Mg, Al, Si, S, K, Ca, Fe, and Ni (i.e., for all elements of relevance for spallation reactions in meteorite studies). In addition, as a check for consistency, we also report data for the stone meteorites Jilin and Farmington. Jilin was degassed prior to irradiation, which changed its chemical composition considerably (Table 1; see also Michel et al. 1989); for Farmington, such a degassing before irradiation was not necessary because its noble gas concentrations from the

Table 1. Chemical composition (wt%) of the materials used for building the artificial stone and iron meteoroids and of the meteoritic material used as target.

Element	Gabbro	Iron	Farmington[a]	Troilite[b]	Jilin (degassed)[c]
O	44.12	–	38.6	–	44.0
Na	1.86 ± 0.02	–	0.65[d]	–	0.5
Mg	4.82 ± 0.90	–	15.15	–	15.5
Al	9.85 ± 0.16	–	1.18	–	10.0
Si	26.08 ± 0.40	<0.4	18.96	–	19.3
S	–	–	2.22[d]	36.5	–
Ca	7.55 ± 0.07	–	1.31	–	1.2
Ti	0.126 ± 0.003	–	0.06	–	–
Mn	0.085 ± 0.003	0.5–0.8	0.26	–	–
Fe	5.51 ± 0.08[e]	>99	20.35	63.5	9.3
Co	0.005 ± 0.0003	–	–	–	–
Ni	0.0114 ± 0.0007	–	1.27[d]	–	–
<A>	21.6	55.8	–	–	–
<Z>	10.7	26.0	–	–	–

[a]After von Michaelis et al. (1969).
[b]Troilite (from Cape York iron meteorite) is assumed to be pure, stoichiometric FeS.
[c]From Michel et al. (1989).
[d]Mean values for L chondrites after Mason (1971).
[e]Includes structural iron bands which hold the gabbro hemispheres together.

exposure in space are small compared with the amounts expected from the artificial irradiation (^{3}He <50 × 10^{-10} cm^3 STP/g and ^{21}Ne <5 × 10^{-10} cm^3 STP/g; Kirsten et al. 1963; Zähringer 1966).

Irradiations and Determination of Proton Fluences

Details of the experiments were presented by Michel et al. 1996, Leya 1997, and Leya et al. 2000b. Briefly, the artificial meteoroids were irradiated with 1.6 GeV protons at the Saturne synchrotron at LNS/Saclay. Isotropic irradiation was achieved by a superposition of two perpendicular rotations and two perpendicular translations of the spheres during irradiation. The fluences of primary protons were 1.32 × 10^{14} cm^{-2} for the gabbro sphere and 2.45 × 10^{14} cm^{-2} for the iron sphere. Fluences and their spatial homogeneity were measured via the ^{22}Na activities in Al-foils, which are located in front of the thick targets and take part in both translational movements. Note that all production rates presented here are normalized to a flux of one primary proton per cm^2 and sec.

Rare Gas Measurements

The analyses of the single-element targets Mg, Al, Si, Fe, and Ni were done in Zürich, while those of the chemical compounds, meteoritic material, gases, and targets in glass ampoules were done in Mainz. The cumulative yield of ^{3}He was determined from the increase with time of the ^{3}He concentrations in the targets resulting from the decay of 12.3-yr tritium (^{3}H). As a check for potential losses by diffusion of tritium from the targets during storage, aliquots of some samples were encapsulated in evacuated break-seal ampoules and, about 10 years after irradiation, were analyzed for ^{3}He.

The Mg, Al, Si, Fe, and Ni targets were cleaned in ethanol and distilled water before being loaded into the storage positions of an all-metal (except for a glass window) noble gas extraction system. To release atmospheric surface contamination, the samples were preheated at ~80 °C for 20 hr. Mg and Al were degassed in a Mo crucible held at 1000 °C for 15 min, and Si was held at 1800 °C for 15 min. In the case of Fe and Ni, also degassed at 1800 °C, an Al_2O_3 liner inside the Mo crucible served to prevent the corrosion of the latter.

Gases were first cleaned on a Zr-Ti-getter at 280 °C and then by means of two additional Zr-Al-getters (SAES®) at 300 °C. During the He and Ne analyses, Ar was adsorbed on activated charcoal held at the temperature of boiling nitrogen. When Ar was measured, this was done separately after He and Ne had been pumped off. Sample gas amounts were determined by peak height comparison with signals from known amounts of He, Ne, and Ar, respectively.

Extraction blanks for ^{3}He, ^{4}He, and ^{21}Ne typically were on the order of a few percent or less of sample gas amounts, except in a few instances where the gas amounts were exceedingly small due to losses from the samples by diffusion. Such data are not evaluated further. Corrections for ^{22}Ne, ^{36}Ar, and ^{38}Ar were made via ^{20}Ne and ^{40}Ar, respectively, assuming all blank Ne and blank Ar to have the isotopic composition of atmospheric Ne and Ar, respectively. For the Ar isotopes, in particular, blank corrections were substantial in almost all cases, reaching up to 75% for the degassed Jilin targets. Measured ^{22}Ne concentrations were, in addition, corrected for a CO_2^{2+} background, yielding an additional uncertainty of <0.5%. Contributions of $^{40}Ar^{2+}$ and $H_2{}^{18}O^+$ to the ^{20}Ne signal were both always below 0.5%.

Uncertainty Analysis

Noble gas concentrations were reproducible to within 2%. The uncertainty of the isotopic ratios is less than 2% in both laboratories. The accuracy of the absolute gas concentrations is ~5%, both for the Zürich and Mainz measurements. An interlaboratory check indicated that the isotopic ratios agree to within 1% (Michel et al. 1989) but that the concentrations measured in the two laboratories differ by 3%, with the concentrations in Mainz being systematically higher than those in Zürich. In the subsequent presentation and discussion, this has been taken into account by arbitrarily reducing the Mainz data by 3%.

Uncertainties of the target mass are always less than 1%. Fluctuations in beam intensities were taken into account when calculating flux densities; they result in an overall uncertainty of less than 1% for the product nuclides discussed here. Interfering reactions from target impurities can be neglected due to the high purity of the foils. Because we always analyzed only the middle one of at least three adjacent target foils of the same element, and because the thickness of all foils exceeded any expected recoil length, recoil losses from the analyzed samples are negligible. The monitor reaction cross section yields an additional uncertainty that affects all data in the same way. This uncertainty, 5% and 7% for the iron and gabbro sphere, respectively, has been added quadratically; it cancels out when discussing production rate ratios.

EXPERIMENTAL RESULTS AND DISCUSSION

Production Rates of ^{4}He, ^{21}Ne, ^{22}Ne, and ^{38}Ar within the Artificial Meteoroids

The production rates for He, Ne, and Ar isotopes from Na, Mg, Al, Si, S, K, Ca, Fe, Ni, and from the meteorite samples of Farmington and Jilin are compiled in Tables 2–7. For the multi-element targets Na_2WO_4, Na_2MoO_4, K_2MoO_4, and $CaMoO_4$, the production rates of ^{4}He are given per gram of chemical compound, while the yields of Ne and Ar are given per gram of target element (Na, K, Ca) assuming that the other constituents of the compounds (O, Mo, W) have contributed insignificantly or, in the case of oxygen, have not contributed at all.

Table 2. Production rates (10^{-10} cm^3 STP/[g × Myr]) for irradiation in the gabbro sphere, normalized to a flux of primary protons of 1 proton per cm^2 and sec.[a]

Target	Depth (mm)	^3He_d	^4He	^{21}Ne	$^{20}Ne/^{21}Ne$	$^{22}Ne/^{21}Ne$	^{38}Ar	$^{36}Ar/^{38}Ar$	$^{39}Ar/^{38}Ar$
Na[b]	32	*(8.8)*	–	29.3	(≡0.9)	2.07	–	–	–
	123	*(5.4)*	–	30.9	(≡0.9)	2.23	–	–	–
	183	*(8.1)*	–	35.9	(≡0.9)	2.11	–	–	–
Mg	21	19.1	182	24.4	0.93	1.11	–	–	–
	38	18.9	202	29.0	–	1.06	–	–	–
	73	21.4	214	32.2	0.89	1.06	–	–	–
	88	–	215	30.6	0.97	1.09	–	–	–
	124	20.8	223	34.4	0.88	1.04	–	–	–
	140	20.9	234	34.5	0.92	1.05	–	–	–
	174	20.2	237	34.0	0.91	1.06	–	–	–
	190	21.0	237	36.9	0.88	1.02	–	–	–
	224	21.7	238	36.4	–	1.03	–	–	–
	243	21.1	238	35.4	0.88	1.05	–	–	–
Al	19	17.3	–	12.2	–	1.20	–	–	–
	36	17.9	163	12.9	0.91	1.21	–	–	–
	70	18.7	–	14.3	–	1.22	–	–	–
	86	18.7	181	14.3	0.95	1.22	–	–	–
	122	18.4	180	14.8	0.95	1.24	–	–	–
	137	18.5	185	15.3	0.86	1.21	–	–	–
	172	18.4	192	15.4	0.91	1.25	–	–	–
	188	18.5	187	15.5	0.86	1.23	–	–	–
	222	18.7	–	15.7	–	1.25	–	–	–
	240	18.6	187	15.6	0.86	1.22	–	–	–
Si	12	18.5	155	9.0	1.06	1.16	–	–	–
	34	–	174	10.1	1.06	1.16	–	–	–
	85	20.0	182	10.8	1.06	1.18	–	–	–
	113	20.1	187	11.3	1.05	1.15	–	–	–
	135	20.0	189	11.4	1.07	1.17	–	–	–
	163	19.7	188	11.2	1.07	1.17	–	–	–
	186	–	190	11.3	1.06	1.19	–	–	–
	214	19.0	191	11.3	1.07	1.18	–	–	–
	236	20.7	198	11.9	1.06	1.16	–	–	–
S[b, c]	41	19.8	163	5.03	1.00	1.07	–	–	–
	56	21.7	139	5.28	1.03	1.14	–	–	–
	91	24.7	221	5.53	0.99	1.12	–	–	–
	107	21.2	207	5.28	0.99	1.13	–	–	–
	142	20.9	196	5.60	1.05	1.13	–	–	–
	146	19.8	226	5.85	1.01	1.12	–	–	–
	156	21.4	215	5.41	1.14	1.12	–	–	–
	192	23.6	234	5.72	1.06	1.09	–	–	–
	197	22.6	226	5.47	0.99	1.16	–	–	–
	207	22.0	177	5.66	1.04	1.11	–	–	–
K[b]	27	*(0.7)*	*(7.0)*	1.43	(≡0.88)	1.57	52.5	0.114	0.49
	40	*(0.5)*	*(7.0)*	1.72	(≡0.88)	1.47	57.7	0.108	0.51
	78	*(0.9)*	*(9.3)*	1.80	(≡0.88)	1.35	62.8	0.115	0.55
	90	*(0.7)*	*(4.6)*	1.79	(≡0.88)	1.29	65.3	0.119	0.56
	128	*(0.5)*	*(4.6)*	1.57	(≡0.88)	1.37	69.2	0.121	0.57
	139	*(0.7)*	*(9.3)*	1.81	(≡0.88)	1.34	69.4	0.103	0.61
	178	*(0.5)*	*(9.3)*	1.51	(≡0.88)	1.60	67.7	0.124	0.61
	190	*(0.9)*	*(7.0)*	1.58	(≡0.88)	1.31	71.1	0.119	0.59
Ca[b]	15	(20.6)	(161)	2.39	(≡0.88)	1.28	31.3	0.422	0.13
	65	(21.1)	(176)	2.24	(≡0.88)	1.30	37.8	0.414	0.13
	115	(21.1)	(217)	2.24	(≡0.88)	1.20	40.7	0.416	0.14

Table 2. Production rates (10^{-10} cm^3 STP/[g × Myr]) for irradiation in the gabbro sphere, normalized to a flux of primary protons of 1 proton per cm^2 and sec.[a] *Continued.*

Target	Depth (mm)	^3He_d	^4He	^{21}Ne	$^{20}Ne/^{21}Ne$	$^{22}Ne/^{21}Ne$	^{38}Ar	$^{36}Ar/^{38}Ar$	$^{39}Ar/^{38}Ar$
Ca	165	(20.6)	(192)	2.24	(≡0.88)	1.10	43.2	0.402	0.13
Fe	7	8.2	108	0.42	–	–	2.39	–	–
	28	9.4	91	0.49	–	–	2.00	–	–
	57	8.6	94	0.40	–	–	1.93	–	–
	79	9.4	99	0.46	–	–	1.95	–	–
	107	9.5	106	0.44	–	–	2.16	–	–
	129	9.3	104	0.44	–	–	1.64	–	–
	158	–	136	0.44	–	–	1.23	–	–
	180	9.2	96	0.42	–	–	1.86	–	–
	208	8.9	100	0.41	–	–	2.19	–	–
	230	8.9	97	0.40	–	–	1.72	–	–

[a]Numbers in brackets are concentrations per gram of multi-element target. Numbers in italics indicate strong losses by diffusion.
[b]Multi-element target.
[c]Corrected for ingrowth of ^{3}He from radioactive decay of ^{3}H assuming P(^{3}H from FeS) = 1.3 P[(^{3}He)$_d$ from FeS] and for the contribution from Fe of the single-element data of this irradiation.

Table 3. Production rates (10^{-10} cm^3 STP/[g × Myr]) for irradiation in the iron sphere, normalized to a flux of primary protons of 1 proton per cm^2 and sec.

Target	Depth (mm)	^3He_d	^4He	^{21}Ne	$^{20}Ne/^{21}Ne$	$^{22}Ne/^{21}Ne$	^{38}Ar	$^{36}Ar/^{38}Ar$	$^{39}Ar/^{38}Ar$
Mg	2	18.6	168	23.9	0.80	1.02	–	–	–
	17	21.1	202	31.0	0.83	0.98	–	–	–
	32	20.9	217	35.0	0.79	0.95	–	–	–
	43	–	223	37.4	0.78	0.92	–	–	–
	61	20.0	221	35.6	0.77	0.94	–	–	–
	76	18.3	223	38.4	0.77	0.93	–	–	–
Al	5	16.9	156	10.4	0.71	1.26	–	–	–
	20	18.2	169	12.2	0.69	1.27	–	–	–
	35	18.3	174	13.3	0.68	1.26	–	–	–
	49	18.4	181	13.8	0.69	1.28	–	–	–
	64	18.1	178	13.9	0.69	1.29	–	–	–
	79	17.7	179	14.0	0.72	1.29	–	–	–
Si	7	19.0	154	8.2	0.86	1.16	–	–	–
	22	19.9	170	9.2	0.90	1.17	–	–	–
	37	20.2	181	9.9	0.89	1.17	–	–	–
	51	20.1	184	10.1	0.91	1.21	–	–	–
	66	19.8	184	10.2	0.90	1.21	–	–	–
	81	19.7	187	10.3	0.90	1.18	–	–	–
S[a, b]	13	18.6	–	4.59	(≡0.83)	1.11	–	–	–
	24	21.9	–	5.15	(≡0.83)	1.12	–	–	–
	45	21.0	–	5.46	(≡0.83)	1.13	–	–	–
	50	21.3	–	5.22	(≡0.83)	1.14	–	–	–
	66	21.7	–	5.57	(≡0.83)	1.12	–	–	–
Ca[a]	14	(23.6)	(160)	2.25	1.35	1.26	32.5	0.43	0.15
	26	(22.3)	(175)	2.25	1.04	0.92	39.2	0.42	0.14
	42	(23.7)	(186)	2.31	1.00	1.00	41.0	0.43	0.14
	59	(24.5)	(193)	2.18	1.07	1.08	43.9	0.42	0.16
	72	(25.0)	(197)	2.18	1.06	1.09	44.6	0.42	0.17
Fe	1	–	84.0	0.52	(≡0.90)	1.07	2.20	0.125	–
	2	10.6	81.0	0.41	(≡0.90)	1.01	1.93	0.125	–
	9	11.7	88.5	0.45	(≡0.90)	1.06	2.21	0.140	0.99
	10	11.4	75.7	0.50	(≡0.90)	1.09	2.04	0.128	0.94
	13	11.5	93.6	0.44	(≡0.90)	1.08	2.29	0.133	–

Table 3. Production rates (10^{-10} cm^3 STP/[g × Myr]) for irradiation in the iron sphere, normalized to a flux of primary protons of 1 proton per cm^2 and sec. *Continued.*

Target	Depth (mm)	^3He_d	^4He	^{21}Ne	$^{20}Ne/^{21}Ne$	$^{22}Ne/^{21}Ne$	^{38}Ar	$^{36}Ar/^{38}Ar$	$^{39}Ar/^{38}Ar$
Fe	18	–	89.2	0.48	(≡0.90)	1.03	2.12	0.125	–
	31	11.4	91.3	0.47	(≡0.90)	1.09	2.27	0.122	0.99
	39	11.8	93.5	0.45	(≡0.90)	1.08	2.26	0.128	0.99
	39	–	96.5	0.46	(≡0.90)	0.99	2.21	0.126	–
	42	11.7	132.8	0.46	(≡0.90)	1.07	2.32	0.132	0.95
	50	11.6	101.1	0.45	(≡0.90)	1.08	2.29	0.128	0.99
	51	11.6	96.5	0.44	(≡0.90)	1.07	2.27	0.133	0.95
	60	–	93.8	0.45	(≡0.90)	1.00	2.19	0.126	–
	60	11.2	88.8	0.42	(≡0.90)	1.04	2.16	0.132	–
	73	–	97.0	0.43	(≡0.90)	1.00	2.20	0.120	–
	80	11.1	98.6	0.43	(≡0.90)	1.10	2.25	0.125	0.99
	95	–	99.1	0.45	(≡0.90)	0.98	2.30	0.126	–
Ni	6	10.9[c]	88.7	0.33	(≡0.90)	0.96	1.55	0.181	–
	22	12.5	99.4	0.37	(≡0.90)	0.94	1.74	0.177	–
	43	12.7	103.2	0.35	(≡0.90)	0.97	1.74	0.177	–
	65	12.2	106.7	0.34	(≡0.90)	0.96	1.78	0.178	–
	69	13.1	109.3	0.35	(≡0.90)	0.96	1.73	0.179	–
	77	12.8	106.0	0.34	(≡0.90)	0.92	1.70	0.176	–
	85	12.2	106.6	0.34	(≡0.90)	0.88	1.70	0.176	–
	97	12.9	107.6	0.34	(≡0.90)	0.99	1.78	0.178	–

[a]Multi-element target.
[b]Corrected for ingrowth of ^3He from radioactive decay of ^3H assuming P(^3H from FeS) = 1.3 P[($^3He)_d$ from FeS] and for the contribution from Fe the single-element data of this irradiation.
[c]Corrected for ingrowth of ^3He and diffusive losses of ^3H using P(^3H)/P(^3He) and D/λ values of Fe targets.

Table 4. Production rates (10^{-10} cm^3 STP/[g × Myr]) in meteoritic material irradiated in the gabbro and iron spheres, respectively, normalized to a flux of 1 primary proton per cm^2 and sec.

Matrix	Meteorite	Depth (mm)	^3He_d	^4He	^{21}Ne	$^{20}Ne/^{21}Ne$	$^{22}Ne/^{21}Ne$	^{38}Ar	$^{36}Ar/^{38}Ar$
Gabbro	Jilin	22	23.2	181	8.0	(≡0.90)	1.13	0.79	0.33
		52	22.5	211	9.2	(≡0.90)	1.11	0.95	0.55
		72	23.5	219	9.3	(≡0.90)	1.10	0.88	0.43
		103	23.5	234	9.2	(≡0.90)	1.14	0.93	0.39
		121	24.0	235	9.8	(≡0.90)	1.09	0.88	0.38
		152	22.7	218	10.1	(≡0.90)	1.12	0.97	0.45
		172	21.6	222	10.2	(≡0.90)	1.10	0.97	0.31
		203	23.2	213	10.7	(≡0.90)	1.09	0.95	0.52
	Farmington	5	17.6	–	5.9	(≡0.90)	1.11	–	–
		23	21.1	–	6.9	(≡0.90)	1.16	–	–
		59	22.3	–	8.2	(≡0.90)	1.11	–	–
		73	21.3	–	8.2	(≡0.90)	1.07	–	–
		109	21.6	–	8.9	(≡0.90)	1.09	–	–
		124	21.1	–	8.7	(≡0.90)	1.10	–	–
		159	21.7	–	8.9	(≡0.90)	1.08	–	–
		174	21.3	–	8.7	(≡0.90)	1.13	–	–
		209	22.2	–	9.1	(≡0.90)	1.11	–	–
		225	20.9	–	8.9	(≡0.90)	1.11	–	–
Iron	Jilin	6	17.4	157	6.8	(≡0.90)	1.07	0.77	0.40
		18	19.0	185	8.5	(≡0.90)	1.05	0.92	0.48
		36	21.3	224	10.6	(≡0.90)	1.02	0.92	0.67
		54	21.1	235	11.0	(≡0.90)	0.99	1.14	0.71
		70	21.0	239	10.8	(≡0.90)	1.01	1.09	0.50

Table 5. Maximum production rates (10^{-10} cm^3 STP/[g × Myr]) for ^4He, $^{20,21,22}Ne$, and $^{36,38,39}Ar$ in target elements irradiated within the gabbro and the iron spheres, respectively, normalized to a flux of primary protons of 1 proton per cm^2 and sec.

Matrix	Target	^4He	^{21}Ne	$^{20}Ne/^{21}Ne$	$^{22}Ne/^{21}Ne$	^{38}Ar	$^{36}Ar/^{38}Ar$	$^{39}Ar/^{38}Ar$
Gabbro	O[a]	276	–	–	–	–	–	–
	Na	–	33.4	(≡0.90)	2.14	–	–	–
	Mg	237	35.3	0.91	1.06	–	–	–
	Al	188	15.4	0.90	1.23	–	–	–
	Si	190	11.4	1.06	1.17	–	–	–
	S	200	5.57	1.04	1.12	–	–	–
	K	–	1.68	(≡0.88)	1.41	69.4	0.115	0.561
	Ca	–	2.24	(≡0.88)	1.22	42.0	0.414	0.132
	Fe	100	0.424	–	–	1.91	–	–
	Jilin (measured)	225	10.0	–	1.11	0.94	0.423	–
	Jilin (calculated)	–	9.45	–	1.13	0.82	–	–
	Farmington (meas.)	–	8.9	–	1.07	–	–	–
	Farmington (calc.)	–	8.1	–	1.11	0.92	–	–
Iron	O[a]	294	–	–	–	–	–	–
	Mg	222	37.1	0.79	0.96	–	–	–
	Al	179	13.9	0.70	1.28	–	–	–
	Si	184	10.2	0.89	1.12	–	–	–
	S	–	5.42	–	–	–	–	–
	Ca	–	2.22	–	1.07	43.2	0.424	0.152
	Fe	96.4	0.443	–	1.05	2.25	0.128	0.974
	Ni	106.6	0.344	–	0.95	1.74	0.178	–
	Jilin (measured)	228	10.5	–	1.03	1.05	0.540	–
	Jilin (calculated)	–	9.35	–	1.06	0.87	–	–

[a]Calculated from Jilin (see Table 7 and text).

Table 6. ^3He_d and ^3H production rates (10^{-10} cm^3 STP/[g × Myr]) and the (dimensionless) ratio D/λ for Mg, Al, Si, Fe, and Jilin samples irradiated within the gabbro sphere. Production rates are for a flux of one primary proton per cm^2 and sec. Entries for $P(^3He)_d$ from Mg, Al, Si, and Fe are averages of the data in Table 2 and those for the "vacuum-sealed" target aliquots.

Target	D/λ	$P(^3He)_d$	$P(^3H)/P(^3He)_d$	$P(^3H) + P(^3He)_d$	$^4He/^3He_{cum}$
O	(≡0)	29.3 ± 3.1	0.73 ± 0.30	50.7 ± 9.0	5.4 ± 0.7
Mg	2.6 ± 0.4	20.5 ± 1.2	(>0.64)	>33.6	<7.1
Al	0.16 ± 0.02	18.2 ± 1.1	1.28 ± 0.07	41.5 ± 2.1	4.53 ± 0.40
Si	0.014 ± 0.001	19.6 ± 1.1	1.16 ± 0.04	42.3 ± 2.1	4.49 ± 0.23
Fe	2.4 ± 1.0	9.5 ± 1.0	(>0.42)	>13.5	<7.4
Jilin	(≡0)	22.7 ± 1.2	0.97 ± 0.15	44.7 ± 3.6	5.03 ± 0.30
Jilin, 600 MeV, 15 cm	(≡0)	11.0 ± 0.6	0.84 ± 0.10	20.2 ± 1.3	5.25 ± 0.75
Jilin, 600 MeV, 25cm	(≡0)	9.0 ± 0.5	0.87 ± 0.13	16.8 ± 1.3	5.88 ± 0.30
Jilin (Iron)	(≡0)	21.0 ± 1.2	1.35 ± 0.26	49.3 ± 5.6	4.62 ± 0.30

For S as the target element, irradiated as FeS and FeS_2, respectively, all yields were corrected for the contributions from Fe as they were determined from the single-element Fe targets in the same irradiations. The corrections amount to ~45% for ^4He in meteoritic FeS and some 7% and 12%, respectively, for spallogenic Ne (^4He in commercial FeS_2 was compromised by high blanks). Some of the production rates are shown in Figs. 1–3. The results of the model calculations also depicted in these figures will be discussed in the Model Calculations section. The production rates for ^3H and ^3He are given in the Isotope Production Rate Ratios section.

^4He is essentially an evaporation product from the final stages of the nuclear reaction; its production rate shows only a minor dependence on the mass number of the target element. Between O, Mg, Al, and Si in both artificial meteoroids, the ^4He production rates vary by less than 50%. The range is reduced even further when looking at the production rates per target *atom*, which are obtained when multiplying the production rates *per gram* by the atomic weight of the target element. Moreover, the ^4He production rates for all target elements in both artificial meteoroids show a similar depth dependence (Tables 2 and 3; Fig. 1).

Table 7. Production rates, in units of 10^{-10} cm^3 STP/g/Myr for a primary flux of 1 proton per cm^2 and sec, of ^3He_d and ^3H from oxygen as a function of depth (mm) inside the iron and gabbro spheres, respectively. Entries for the contributions to the total production rate of the sum of all elements except oxygen are per gram of meteorite ($P_{non\text{-}oxygen}$). Those for oxygen pertain to gram oxygen. The elemental production rates are from Table 6, and chemical compositions are from Table 1.

Matrix	Meteorite	Depth (mm)	$P(^3He)_d$[a]	$P(^3He)_d$ non-oxygen	$P(^3He)_d$ oxygen	$P(^3H)$	$P(^3H)$ non-oxygen	$P(^3H)$[b] oxygen	$P(^3H)/P(^3He)_d$ oxygen	$P(^3H) + P(^3He)_d$ oxygen
Gabbro	"Jilin"	22*	23.2	9.6	31.0	22.5	12.3	23.2	0.75	54.2
		52	22.5	10.1	28.1	21.8	12.9	20.2	0.72	48.3
		72	23.5	10.1	30.5	22.8	12.9	22.5	0.74	53.0
		103	23.5	10.1	30.5	22.8	12.9	22.5	0.74	53.0
		121	24.0	10.1	31.5	23.3	12.9	23.5	0.75	55.0
		152[c]	22.7	10.1	28.6	22.0	12.9	20.7	0.72	49.3
		152[c]	22.7	10.1	28.7	22.0	12.9	20.7	0.72	49.4
		172	21.6	10.1	26.2	21.0	12.9	18.3	0.70	44.5
		203	23.2	10.1	29.8	22.5	12.9	21.8	0.73	51.6
Average without*			23.0	10.1	29.2	22.3	12.9	21.3	0.73	50.5
Gabbro	Farmington	5*	17.6	9.3	21.3					
		23*	21.1	9.7	29.6					
		58	22.3	10.0	31.6					
		73	21.3	10.2	28.6					
		109	21.6	10.2	29.6					
		124	21.1	10.2	28.3					
		159	21.7	10.2	29.8					
		174	21.3	10.2	28.7					
		209	22.2	10.2	31.2					
		225	20.9	10.2	27.8					
Average without*			21.6	10.2	29.4					
Iron	"Jilin"	5.9*	17.4	9.6	17.6					
		18.0*	19.0	10.2	19.9					
		35.9	21.3	10.2	25.2					
		54.0	21.1	10.2	24.7					
		69.5[c]	21.0	10.2	24.4					
		69.5[c]	21.0	10.0	25.0					
Average without*			21.1	10.2	24.8					

[a]Entries from Table 4, column 4.
[b]Elemental production rates: Isotope Production Rate Ratios section.
[c]In two instances, degassed Jilin targets from the same depth during irradiation are listed. They are based on independent measurements performed several years apart.

^{21}Ne and ^{22}Ne from Na, Mg, Al, and Si are essentially low-to-medium energy products. This is clearly seen in the production rates that increase from surface to center by ~25% to ~45% (Tables 2 and 3; Fig. 2). Production rates increasing with depth are also observed for ^{21}Ne and ^{22}Ne in Jilin and Farmington (Table 4) because, in these multi-element targets, the production rates are dominated by reactions on Mg, Al, and Si. With increasing target mass number, the depth profiles become flatter; for S, K, Ca, Fe, and Ni, there is no systematic trend discernible.

The depth dependence of the production rate of ^{38}Ar from Ca is very much the same as that of $P(^{21}Ne)$ from Mg. Hence, there is no change with depth of the ratio of the two production rates with mean $P(^{38}Ar)_{Ca}/P(^{21}Ne)_{Mg}$ values of 1.14 ± 0.03 and 1.24 ± 0.03 for the iron sphere and the gabbro sphere, respectively. Both results, the constancy of the ratio with depth and its value being close to unity, agree with what has been observed in a suite of 12 mesosiderites that for a more than tenfold variation of the absolute production rates, yielded an average $P(^{38}Ar)_{Ca}/P(^{21}Ne)_{Mg}$ of 1.04 ± 0.10 (Begemann et al. 1976).

In Fig. 3, we have plotted ^{38}Ar production rates from Fe. The data from the gabbro sphere scatter too much to recognize any trend, while those for the iron sphere suggest a slight increase with depth of the production rate. For K and Ca, the ^{38}Ar production rates increase from the surface of the gabbro sphere toward its center by ~30% (Tables 2 and 3), reflecting that ^{38}Ar from these elements is a low-to-medium energy product. There is no trend for the ^{38}Ar production from Ni.

Inspection of the individual depth profiles shows that the production rates increase up to a depth of ~10 cm in the gabbro sphere and 4 cm in the iron sphere, i.e., up to a depth

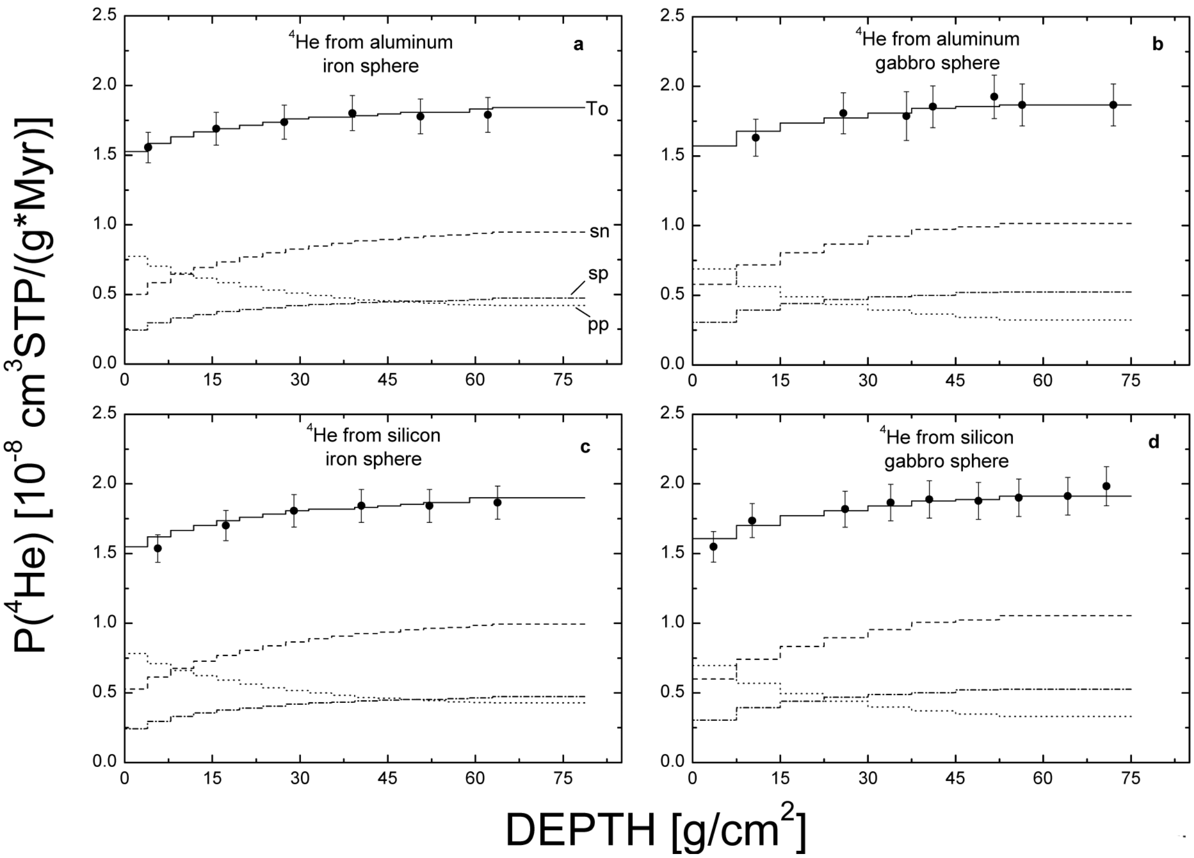

Fig. 1. Experimental (dots) and calculated (lines) production rates of ^{4}He from Al and Si irradiated within an iron and a gabbro sphere, respectively. For the calculated data, the total production (To) and the contributions by primary protons (pp), secondary protons (sp), and secondary neutrons (sn) are distinguished. All data are normalized to $J_{0,\,pp} = 1$ cm^{-2} s^{-1}. For the conversion of the irradiation depths, in mm, to g/cm^2, densities of $\rho = 3.0$ g × cm^{-3} and $\rho = 7.86$ g × cm^{-3} for gabbro and Fe have been used, respectively.

within the meteoroids of ~30 g/cm^2 in both cases. Although our dummy meteoroids were too small to show it, at greater shielding, the production rates will, of course, decrease again. In Table 5, we have compiled the maximum production rates of ^{4}He, ^{21}Ne, and ^{38}Ar from all target elements. For ^{21}Ne and ^{38}Ar, we observe the expected steep dependence on ΔA—the difference in mass between target mass A_0 and product mass A. According to Geiss et al. (1962), in meteorites exposed to the cosmic radiation, the total isobaric spallation yields can be written as:

$$P(A_0, \Delta A) = \text{const.} \times A_0^{2/3} \times (\Delta A)^{-n} \tag{1}$$

where the "irradiation hardness index" *n* is a measure for the ratio of high-energy nuclear-active particles to medium-energy, nuclear-active particles. For the case in which the differential energy spectrum of the cosmic radiation follows a power law:

$$f(E)dE = f_0 \times E^{-\alpha}dE \tag{2}$$

the hardness index *n* is related to the exponent α in the energy spectrum by $n = ½(3\alpha - 1)$, i.e., a low value of n corresponds with a "hard" irradiation, and a large value of n corresponds with a "soft" irradiation. To determine the irradiation hardness index, the yield ratio of two spallation products (^{21}Ne and ^{38}Ar) produced from the same target element (Fe, Ni) is most commonly used, in which case:

$$P(\Delta A_1)/P(\Delta A_2) = (\Delta A_1/\Delta A_2)^{-n} \tag{3}$$

In their comprehensive study of iron meteorites, Voshage and Feldmann (1979) report ^{38}Ar/^{21}Ne ratios between 3.71 and 5.91, corresponding to n values between 1.98 and 2.69, with a pronounced clustering around n = 2.3 (Fig. 4). In different pieces of metal from the Brenham pallasite, Honda et al. (2002) found 4.55 ≤^{38}Ar/^{21}Ne ≤7.0, which translates into n values up to 2.9, while Nyquist et al. (1973) found n values between 1.85 and 2.25 for the metal phase from chondrites (5 Hs, 9 Ls, 2 LLs). The latter authors suggest that the low values for stone meteorites are essentially a matter of size and that, on average, stone meteorites have been exposed to a harder irradiation because they are smaller in mass than average iron meteorites. This is supported by the results of the very large stone meteorite Jilin where a number of metal nuggets have yielded much higher n values that almost equate

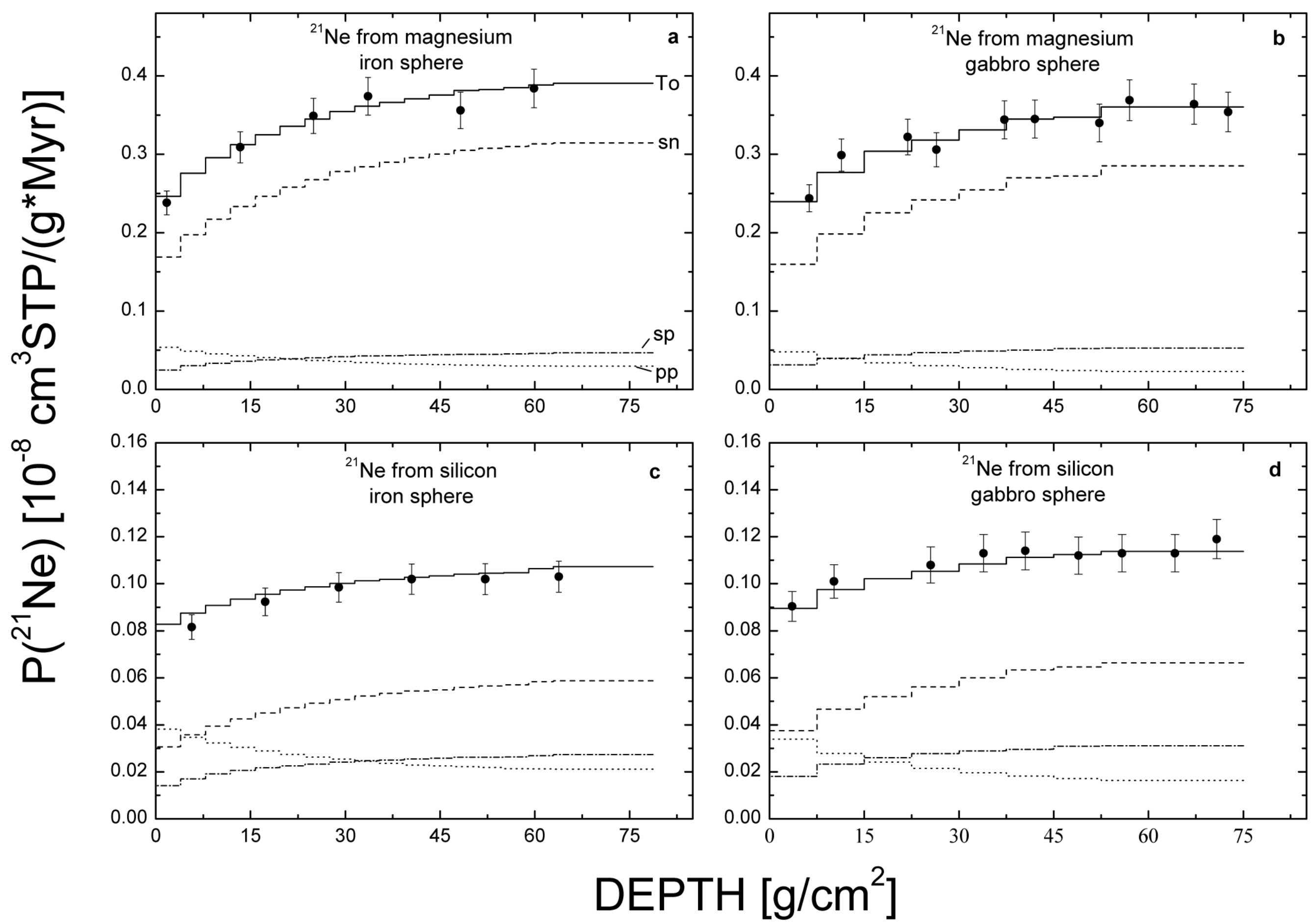

Fig. 2. Experimental and calculated production rates of ^{21}Ne from Mg and Si irradiated within an iron and a gabbro sphere, respectively. The symbols are as in Fig. 1. For a further explanation, see Fig. 1.

with those in metal from the large-mass pallasite Brenham (Begemann et al. 1985, 1996). Comparatively, the present data for Fe targets irradiated in the gabbro sphere give n = 2.25, while for Fe targets irradiated in the iron sphere, n = 2.43.

Another way to derive the irradiation hardness index from Equation 1 is to compare the production yields of the same spallation product from different target elements (Fig. 5), i.e., to evaluate:

$$P(A_{0,1}, \Delta A_1)/P(A_{0,2}, \Delta A_2) = (A_{0,1}/A_{0,2})^{2/3} \times (\Delta A_1/\Delta A_2)^{-n} \quad (4)$$

Using the ^{21}Ne maximum production rates from target elements Mg to Fe (Ni in the case of the iron sphere) yields a best-fit of n = 2.09 for the gabbro sphere and n = 2.15 for the iron sphere. The internal consistency of the results from the two approaches is as good as one might expect. Moreover, these values indicate that as far as spallation systematics are concerned, an irradiation with 1.6 GeV primary protons is a fairly realistic approximation of natural conditions in space. Nevertheless, the production rates given in Tables 2–5 do not necessarily apply to meteorites exposed to the cosmic radiation with its wide energy spectrum. These "meteoritic" production rates are most reliably obtained by model calculations that use data from realistic simulation experiments. Some results of those model calculations have already been published by Leya et al. (2000a, 2001).

There is one notable result in the target data that is worth emphasizing. Presently, the most widely quoted compilations of the relative importance of individual target elements for the production of ^{21}Ne in meteorites (Eugster 1988; Eugster and Michel 1995) list P_{Mg}:P_{Al}:P_{Si}:P_S:P_{Ca}:P_{FeNi} = 1.63:0.6:0.32:0.22:0.07:0.021 as they were originally deduced by Schultz and Freundel (1985). Normalized to P_{Si}, the numbers are $P_{Mg/Si}$:$P_{Al/Si}$:P_{Si}:$P_{S/Si}$:$P_{Ca/Si}$:$P_{FeNi/Si}$ = 5.1:1.88:1.00:0.69:0.22:0.066. According to the present data for the maximum production rates (Table 5), we find the relative yields to be 3.1:1.35:1.00:0.49:0.20:0.037 for an irradiation within gabbro and 3.6:1.36:1.00:0.53:0.22:0.042 when irradiated within iron. Since all Si-normalized yield factors are smaller, by roughly the same percentage, than the factors obtained from the deconvolution of data from meteorites with different chemical composition (Schultz and Freundel 1985), these meteorite data appear to overestimate the relative yield from

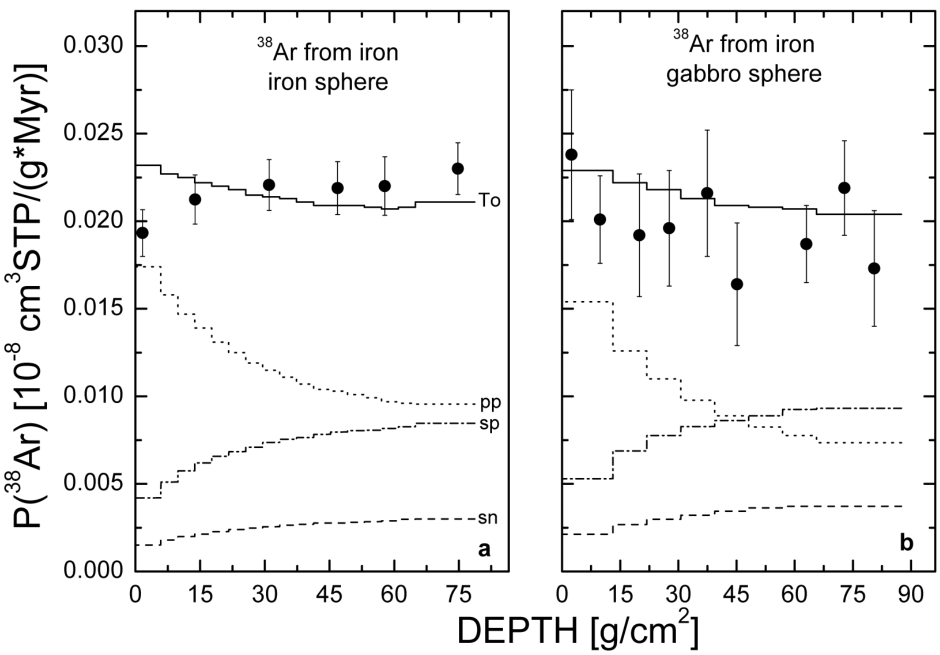

Fig. 3. Experimental and calculated production rates of ^{38}Ar from Fe irradiated within an iron and a gabbro sphere, respectively. The symbols are as in Fig. 1. For further explanation, see Fig. 1.

Si by ~40%. This is confirmed by the model calculations that give average ratios $P_{Mg/Si}$:$P_{Al/Si}$:P_{Si}:$P_{Ca/Si}$:$P_{FeNi/Si}$ = 3.59:1.26: 1.00:0.16:0.026 (note that there is no value for S) for H chondrites with radii from 5 cm up to 120 cm (Leya et al. 2000a).

Isotope Production Rate Ratios

Measured ^{36}Ar/^{38}Ar ratios range from about 0.12, for Ar produced from K and Fe, up to 0.42 for Ca as target element. Note that the ^{38}Ar represents the total mass-38 isobaric yield, while the ^{36}Ar is only the directly produced fraction without any significant contribution from the decay of its isobaric precursor ^{36}Cl ($T_{1/2}$ ≈300,000 yr). Thus, the different measured ^{36}Ar/^{38}Ar ratios do not necessarily indicate large differences between different target elements of the ^{36}Ar/^{38}Ar ratio attained at long exposure times or after complete decay of ^{36}Cl. These differences possibly reflect different distributions of the fractional yields along isobar 36 between ^{36}Ar and ^{36}Cl, as has been found to be the case in meteorites. In mesosiderites, Begemann et al. (1976) found that, for Ca as the target element, ~80% of the total ^{36}Ar is produced directly, and ~20% derives from the radioactive precursor ^{36}Cl, while for Fe as the target element, the isobaric distribution is the opposite with ~80% of the total ^{36}Ar being produced via ^{36}Cl and only ~20% produced directly. Presumably, the same effect also accounts for the different ^{39}Ar/^{38}Ar ratios measured for K, Ca, and Fe (Table 5).

Where ^{20}Ne/^{21}Ne ratios could be measured without being compromised by contamination from atmospheric Ne, small but distinct differences between different target elements (Tables 2, 3, and 5) are evident. In particular, Mg and Al yield spallogenic Ne with a very low ^{20}Ne/^{21}Ne ratio. Moreover, in all cases, the ratios are lower, by 15–30%, upon irradiation of the targets within the iron sphere as compared to being irradiated within the gabbro sphere.

^{22}Ne/^{21}Ne ratios are subject to the same problem previously discussed for ^{36}Ar/^{38}Ar—part of the total isobar-22 yield is held up at radioactive ^{22}Na. Here, the problem is less serious than for ^{36}Cl, however, because the relatively short half-life of ^{22}Na of 2.60 yr makes it feasible to follow the ingrowth of ^{22}Ne from the decay of ^{22}Na. In addition, and as a check, ^{22}Na can be measured conveniently by non-destructive counting analysis. All subsequent ^{22}Ne/^{21}Ne ratios are for the total cumulative yield of ^{22}Ne as it was determined by either or both method(s). Whenever both methods were employed for the same target, the agreement was found to be very good.

Two results are most conspicuous. The ^{22}Ne/^{21}Ne ratio of 2.14 in spallogenic Ne produced from Na is very much higher than in any other target element. This is in qualitative agreement with meteorite data. Smith and Huneke (1975) deduced an even higher ratio of ^{22}Ne/^{21}Ne = 2.9 ± 0.3 for spallogenic Ne produced from Na in "ordinary chondrites." As can be seen from Table 5 (column 4), the ^{21}Ne yield increases when going from Si to Mg but, the trend is reversed for Na. This change in yield systematics for Na suggests that the reason for the high ^{22}Ne/^{21}Ne ratio is, largely, a low yield of ^{21}Ne from Na. The other notable result is the matrix-dependency of the ^{22}Ne/^{21}Ne production ratio from Mg.

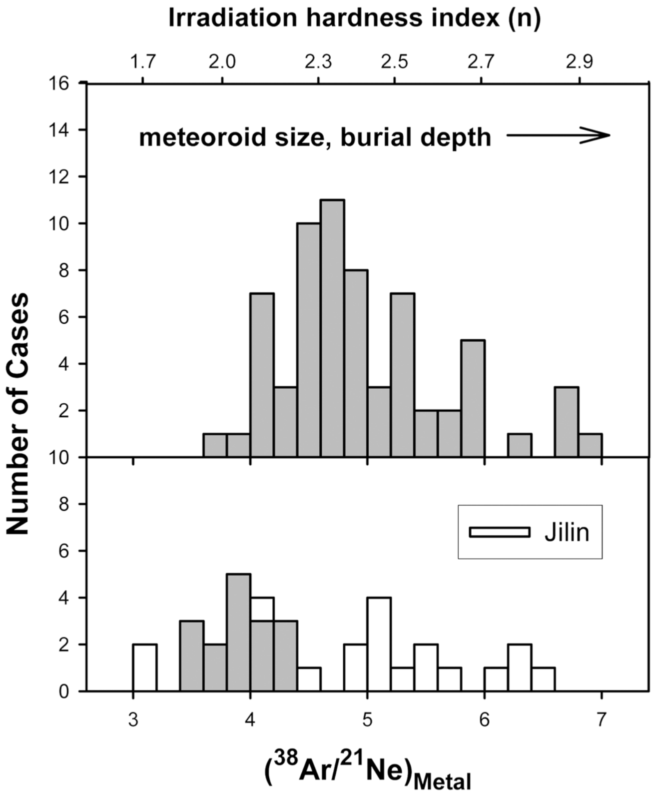

Fig. 4. Irradiation hardness index (n) derived from spallogenic ^{38}Ar/^{21}Ne ratios in iron meteorites (Voshage and Feldmann 1979), a pallasite (Honda et al. 2002) (top panel), and clean metal from chondrites (lower panel; Nyquist et al. 1973) including very large Jilin (Begemann et al. 1985, 1996). The maximum production rates from the present 1.6 GeV irradiation experiment yield n = 2.09 for the gabbro sphere and n = 2.15 for the iron sphere (see Fig. 5).

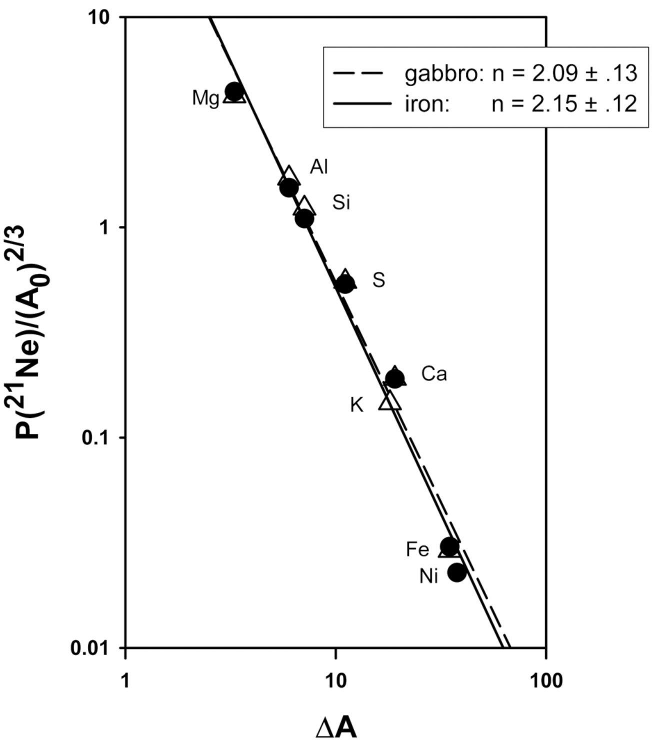

Fig. 5. Normalized ^{21}Ne production rates $P(^{21}Ne)/(A_{target})^{2/3}$ versus mass difference (ΔA) between ^{21}Ne and target mass yield an irradiation hardness index n_{gabbro} = 2.09 (open triangles) and n_{iron} = 2.15 (full dots). The numerical values are the same within the experimental uncertainties of ±0.13.

Irradiation within the iron sphere yields a ratio about 10% smaller than irradiation within the gabbro sphere. The same effect, of just about the same magnitude, has been observed in meteorites by comparing chemistry-normalized Ne isotope data from pallasites/mesosiderites with that from L chondrites (Begemann and Schultz 1988).

For a calculation of reliable cosmic ray exposure ages of meteorites using the isobaric nuclide pair ^{3}H–^{3}He, the production ratio $P(^{3}He)_d/P(^{3}H)$ must be known to take into account the fraction $^{3}He_d$ of the total $^{3}He_{cum}$, which did not originate via the radioactive decay of tritium (^{3}H) but was produced directly as ^{3}He: $P(^{3}He)_{cum} = P(^{3}H)\ [1 + P(^{3}He)_d/P(^{3}H)]$. There are two lines of evidence bearing on this issue. First, there is a wealth of target data where thin metal foils were irradiated with mono-energetic protons ranging in energy up to 25 GeV. (For a compilation of data, see Kirsten and Schaeffer [1971].) Secondly, there are also results from noble gas studies on meteorites that are of more immediate relevance. In a number of iron meteorites, hexaedrites in particular, spallogenic ^{3}He/^{4}He, ^{3}He/^{21}Ne, and ^{3}He/^{38}Ar abundance ratios are encountered that are much lower than normal. Hintenberger and Wänke (1964) were the first to argue that these abnormal ratios are not due to any peculiarities of the irradiation conditions but reflect the loss in space of tritium before it had a chance to decay to ^{3}He. Quantitatively, it was concluded that, in iron meteorites with Ni between 5 and 6%, the production rate ratio should be $P(^{3}H)/P(^{3}He)_d = 2.0 \pm 0.3$ (Hintenberger et al. 1967).

Perhaps more puzzling in this connection was the observation that all freshly fallen iron meteorites contained less tritium than expected from spallation systematics (Fireman and DeFelice 1960; Bainbridge et al. 1962), even in such cases where there was no indication from the relevant nuclide abundance ratios, like ^{3}He/^{4}He, ^{3}He/^{21}Ne, or ^{3}He/^{38}Ar, that losses of tritium had occurred while in space. It appeared that the behavior of tritium changes dramatically during storage of the irons on Earth when, relative to ambient conditions in space, tritium diffusion is accelerated by orders of magnitude. With this in mind, it appeared worthwhile to evaluate the present data in this respect.

In the absence of counting facilities to determine the amount of tritium by its radioactivity, we relied entirely on mass spectrometric noble gas measurements, measuring the increase with time in the targets of the ^{3}He concentration due to the tritium decay ($T_{1/2}$ = 12.3 yr). In principle, two such measurements, separated in time by at least a few years, suffice to determine $P(^{3}H)/P(^{3}He)_d$. The situation is less straightforward if, in addition to the radioactive decay, with decay constant (λ), tritium is lost from the targets by diffusion. However, under the simplifying assumption that such losses also follow a simple exponential law, with a constant (D) describing these losses by diffusion, only one more, a third, measurement is required for this quantity to be measured as well. As a double check for such diffusive losses, aliquots of the metallic Mg, Al, Si, Fe, and Ni foils were sealed in evacuated glass break-seal ampoules, and the ^{3}He content of the ampoules, together with that of the encapsulated targets, were measured ~10 yr after irradiation. For technical and health hazard reasons, the targets were not available to be encapsulated immediately after the irradiation, so any losses by diffusion during this cooling period of the targets (≈300 d) are not included. Losses during the irradiation itself, when the targets were at an (unknown) elevated temperature, are also not included in such measurements.

The results for P(^{3}H), P(^{3}He), and the ratio D/λ (dimensionless) are compiled in Table 6. In the case of metallic Mg and metallic Fe, we find tritium to be lost at a fast rate. For Fe, this agrees with previous target studies by Dubost and Lefort (1963), Fisher (1967), and Fechtig et al. (1967), who also found that terrestrially produced tritium, spallogenic as well as ^{3}He(n,p)-induced, diffuses from the targets on time scales of months.

In view of the fact that tritium losses from the targets during irradiation (5.2 days for the iron sphere and 11.7 days for the gabbro) and during the cooling period until their encapsulation are not included in our measurements, all tritium and total ^{3}He production rates are lower limits. Actually, the data in Table 6 for the low apparent total ^{3}He$_{cum}$ production rates and the high apparent spallogenic ^{4}He/^{3}He$_{cum}$ production ratios support the result that, for Mg and Fe, such diffusive losses have been serious. For Al and Si, on the other hand, we do not anticipate any major effects; the entries in Table 6 are based on the assumption that no losses have occurred. The same is also assumed for the (degassed) Jilin meteorite targets. Unfortunately, for these samples, the uncertainties in the P(^{3}H)/P(^{3}He)$_d$ production rate ratios are fairly large so that the nominally higher tritium production upon bombardment in the iron sphere, as compared to what is produced within the gabbro, is not significant.

The results obtained on degassed Jilin targets from earlier irradiations by 600 MeV protons are also included in Table 6 (Michel et al. 1989). Aliquots of four samples, irradiated on December 19, 1983 at a depth of between 6.5 cm and 19.5 cm within a 25 cm radius gabbro sphere, were analyzed 1.74 yr and 19.0 yr after irradiation, respectively; four other specimens exposed between 0.6 cm and 11.4 cm depth within a 15 cm radius gabbro sphere on November 22, 1984 were measured 1.06 yr and 18.0 yr later. In the case of thick targets like the present ones, the absolute production rates are, of course, smaller for the 600 MeV irradiation as compared to a primary proton energy of 1.6 GeV; the ratios P(^{3}H)/P(^{3}He)$_d$ and ^{4}He/^{3}He$_{cum}$, however, are much the same for all three irradiations. Since the decay intervals for the tritium ($T_{1/2}$ = 12.3 yr) in the samples from the 600 MeV experiments were much longer than the ~7 yr for the 1.6 GeV irradiation, the accuracy is greatly improved. There is no significant difference in the production rate ratios between 1.6 GeV and 600 MeV; the weighted averages for the three irradiations within gabbro are P(^{3}H)/P(^{3}He)$_d$ = 0.88 ± 0.05 and P(^{4}He)/P(^{3}He)$_{cum}$ = 5.37 ± 0.3. As mentioned above, the uncertainty exists in both ratios of whether or not tritium was lost from the Jilin targets by diffusion. However, the agreement in the P(^{3}H)/P(^{3}He)$_d$ ratios obtained from three sets of noble gas data where the interval for the decay of tritium varied between 7 yr and 19 yr suggests that any such losses have been unimportant. Still, the fairly large uncertainties in the ratios for the 1.6 GeV experiment makes this conclusion less robust than one would like it to be.

In Fig. 6, we have plotted the experimental and the calculated direct, non-cumulative production rates of ^{3}He$_d$ from Mg (a), Al (b), and Si (c) in the 600 MeV gabbro (CERN) experiment and the 1.6 GeV gabbro and iron spheres, respectively. The lower right panel (Fig. 6d) shows ^{3}He$_d$ production rates from Fe for the two 1.6 GeV experiments. The depth profiles for all three experiments and all four target elements are rather flat. Even more importantly, the production rates show no dependence on the bulk chemical composition of the artificial meteoroid (matrix effect, see The Influence of Bulk Chemical Composition on the Production Rates section).

The ^{3}He$_d$ production rates from O were derived by resorting to the ^{3}He concentrations as measured in "Jilin" and Farmington (Table 4) but were corrected for the ingrowth from the decay of tritium up to the time of analysis (~10% for the irradiation in gabbro and ~20% for irradiation in the iron dummy). From these numbers, we subtracted the contributions owing to Mg, Al, Si, and Fe as they follow from the known single-element data of the latter (Tables 2 and 6) and the chemical compositions of irradiated "Jilin" and Farmington as listed in Table 1. Sodium, for which no reliable elemental production rate is available, was assumed to contribute as Mg. Thus, its concentration was added to that of Mg. Likewise, S and Ca were added to Si, and Mn, Ti, Cr, and Ni were pooled with Fe. Altogether, these elements make up ~45% of the total production in Jilin and Farmington. The same procedure was then followed to derive the production rate of ^{3}H using P(^{3}H)/P(^{3}He)$_d$ ratios of 0.97 for Jilin, 1.28 for Al, 1.16 for Si (Table 6), and 1.22 for Mg, which is the average of the Al and Si ratios. For Fe, we used a production rate ratio of 2 (Hintenberger et al. 1967).

The ^{3}He production rates from oxygen are compiled in Table 7 and plotted in Fig. 7. Some of the data are also summarized in the first line of Table 6. Because of the various assumptions entering into the calculations, these numbers have higher uncertainties than those from Al and Si. Since the

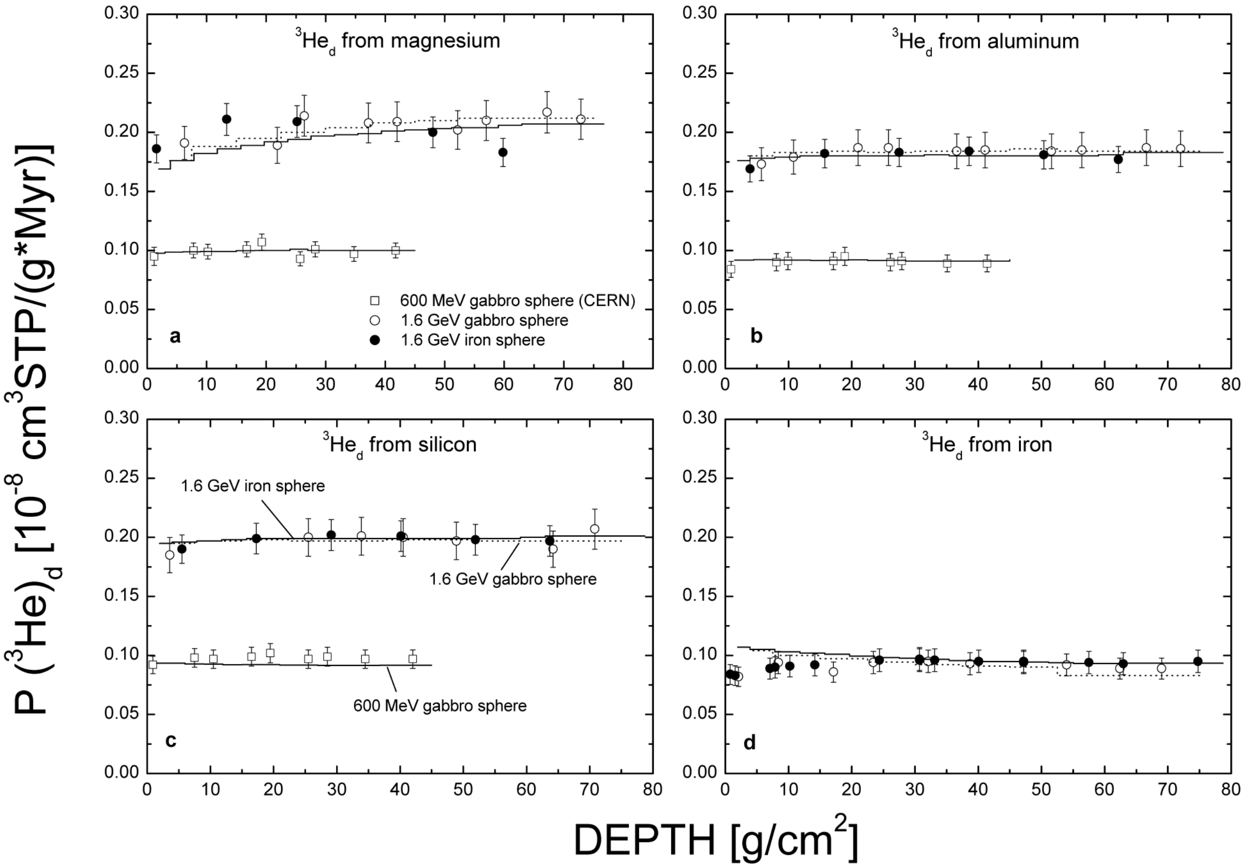

Fig. 6. Experimental and calculated production rates of ^3He_d from Mg (a), Al (b), and Si (c) for the 1.6 GeV gabbro and iron spheres and the 600 MeV CERN experiment (gabbro sphere, 15 cm radius). Panel (d) shows the experimental and measured ^3He production rates for Fe for the two 1.6 GeV experiments. All production rates are normalized to $J_{0, pp} = 1$ cm^{-2} s^{-1}.

$P(^3H)/P(^3He)_d$ ratios for the individual elements are known only for the irradiation within the gabbro dummy, and the ratio for Farmington is not known at all, we did not calculate the production rate ratios for oxygen in these two instances.

The Influence of Bulk Chemical Composition on the Production Rates

The influence of the bulk chemical composition on the elemental production rates, the so called "matrix effect" (Begemann and Schultz 1988), has been discussed for meteorites by Masarik and Reedy (1994), Leya (1997), and Albrecht et al. (2000) and, for the simulation experiments, by Leya (1997) and Leya et al. (2000b). As emphasized by these authors, noticeable effects on production rates are limited to products only a few mass units away from the target masses (e.g., ^{58}Co from Ni and ^{54}Mn from Fe). The present data are in accord with this observation. The irradiation hardness index, which is a measure for the ratio of high-energy nuclear-active particles to medium-energy nuclear-active particles, is virtually the same for the gabbro sphere and the iron sphere. Clearly, the small nominal differences, discussed in the Production Rates of ^4He, ^{21}Ne, ^{22}Ne, and ^{38}Ar Within the Artificial Meteoroids section ($n_{gabbro} = 2.25$ and $n_{iron} = 2.43$ derived from the production ratio $^{38}Ar/^{21}Ne$ on Fe as target, and $n_{gabbro} = 2.09$ and $n_{iron} = 2.15$ for ^{21}Ne produced from different target elements) are not significant.

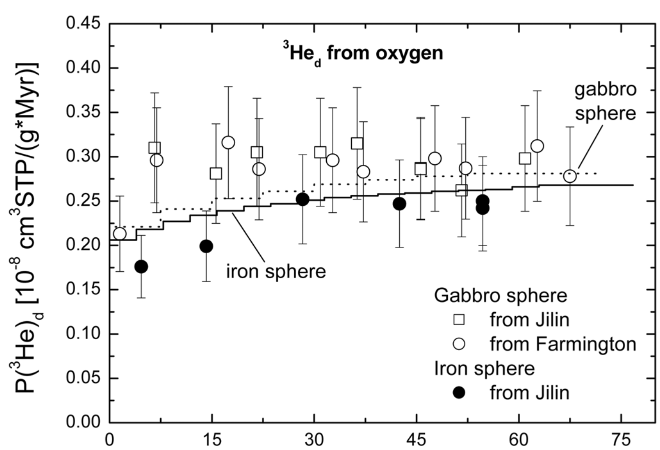

Fig. 7. Experimental and calculated production rates of ^3He_d from O for irradiation within the iron and gabbro sphere, respectively. All production rates are normalized to $J_{0, pp} = 1$ cm^{-2} s^{-1}.

The isotope production ratios of Ne produced from Mg, Al, and Si, on the other hand, show clear effects. Of these, we already have mentioned the lower $^{22}Ne/^{21}Ne$ ratio of spallogenic Ne produced from Mg when irradiated in the iron sphere as compared to Mg irradiated in gabbro (Fig. 8). Even more pronounced is the influence of matrix composition on the $^{20}Ne/^{21}Ne$ ratios. Also, for all three elements (Mg, Al, Si), these ratios are lower by ~15–30% upon irradiation in the iron sphere as compared to irradiation of the targets within gabbro. This can be explained by the dependence on chemical composition of the intranuclear cascades and of particle loss effects (Leya 1997; Leya et al. 2000b). The flux density of secondary neutrons with E <40 MeV is slightly higher in the iron sphere than in the gabbro sphere. In contrast, there are more neutrons with high energy (E >40 MeV) inside the gabbro sphere than in the artificial iron meteoroid (Leya 1997; Leya et al. 2000b). Since ^{22}Ne from Mg and ^{21}Ne and ^{22}Ne from Al and Si are medium energy products, their production rates are slightly higher in the gabbro than in the iron sphere. In contrast, the ^{21}Ne production from Mg is dominated by the (n, α)-reaction on ^{24}Mg, which has a lower reaction threshold than the ^{22}Ne production from Mg and the ^{21}Ne production from Al and Si, respectively. As a consequence, the ^{21}Ne production rates from Mg are similar in both matrices.

MODEL CALCULATIONS

In this section, we compare measured production rates for He, Ne, and Ar isotopes with modeled data based on the strictly physical model described by Michel et al. (1991, 1996), Leya (1997), and Leya et al. (2000b). As discussed in detail by Leya (1997) and Leya et al. (2000b), the production rates from the thick-target experiments provide the basis for an evaluation of the model calculations. Hence, the new data for ^{3}H and the light noble gases presented in this paper allow us to further improve the model calculations for meteoroids and lunar surface material. In this section, we present examples of the ability of the model calculations to describe the depth-, size-, and matrix-dependent production rates in the artificial irradiations, including the data from three 600 MeV simulations with 5 cm, 15 cm, and 25 cm spheres, respectively (Michel et al. 1986, 1989; Dragovitsch 1987; Lüpke 1993; Leya 1997; Leya et al. 2000b). The capability of the model calculations to predict the production rates of the light noble gases in meteoroids and lunar rocks is given in Leya et al. (2000a, 2001).

In Figs. 1, 2, 3, 6, and 7, we compare the measured and modeled production rates for the two 1.6 GeV simulation experiments. In the first three instances, the total production (To) and the contributions by primary protons (pp), secondary protons (sp), and secondary neutrons (sn) are shown separately. For all target-product combinations shown, the measured and modeled data agree within the expected uncertainties, although, the calculated depth profile for ^{38}Ar from Fe, irradiated within the iron sphere, decreases with depth, while the measured depth profile tends to slightly increase from surface to center (Fig. 3). A comparison of the measured and modeled ^{3}He production rates for the two 1.6 GeV experiments and the 600 MeV simulation with a 15 cm sphere is shown in Fig. 6, where only the total modeled production rates $^{3}He_d$ are plotted. Figure 9 presents the ratio of modeled and measured production rates averaged over shielding depths as a function of the relative mass difference between the target and product. The mean value is 1.02 with a standard deviation of 0.12. The outliers for ^{4}He from Mg, Al, and Si for the 25 cm CERN experiment might be due to insufficient blank corrections for these samples. Whether the discrepancies for ^{20}Ne from Al and Si can be explained by an

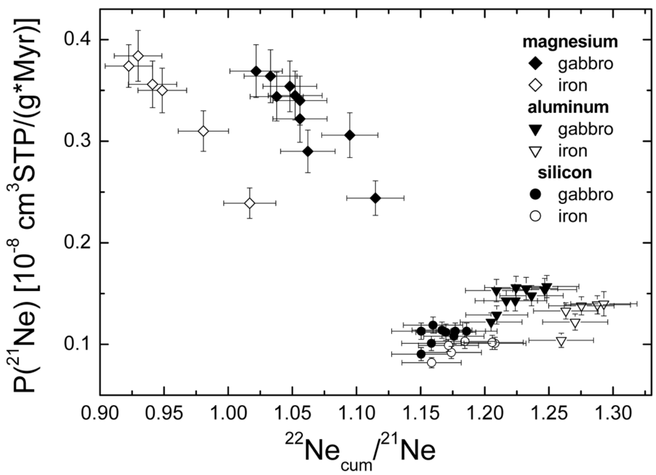

Fig. 8. ^{21}Ne production rates for Mg, Al, and Si as a function of the shielding indicator $^{22}Ne/^{21}Ne$ for the iron (open symbols) and the gabbro spheres (solid symbols). The production rates are normalized to $J_{0, pp} = 1\ cm^{-2}\ s^{-1}$.

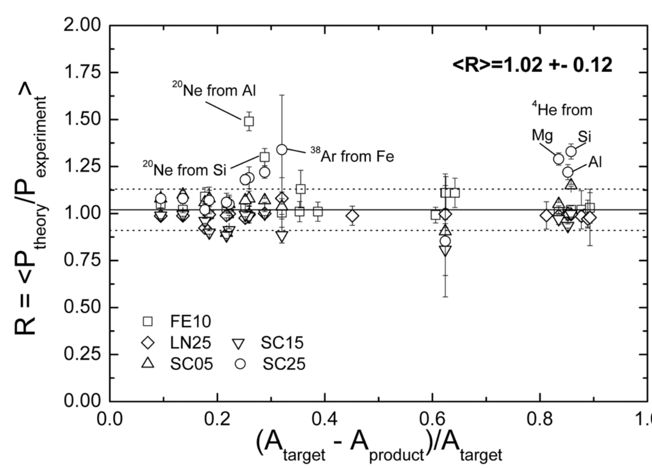

Fig. 9. Ratio of modeled over measured He, Ne, and Ar production rates, from different targets, averaged over shielding depths as a function of the relative target-product mass difference. The symbols indicate five different experiments. The mean value is ~1.02 with a standard deviation of ~0.12.

overestimation of the matrix effect by the model calculations is not yet clear. Also, unrecognized blank problems may serve as an explanation. Fortunately, for the discussion of cosmogenic nuclides in extraterrestrial matter, ^{4}He and ^{20}Ne are not of great importance.

Obviously, the model describes size-, depth-, and matrix-dependent production rates for the light noble gas isotopes in all five simulation experiments simultaneously to within ~12%, which, according to Michel et al. (1996), Leya (1997) and Leya et al. (2000a, b; 2001), also happens to be the uncertainty of the model predictions for meteoroids, lunar surface material, and terrestrial surface samples.

NEW PRODUCTION RATES FOR $^3He_{cum}$ IN STONY METEOROIDS

The meteoritic cumulative $^3He_{cum}$ production rates presented by Leya et al. (2000a) were based on input data that were not corrected for tritium diffusive losses and on assuming $P(^3H)/P(^3He)_d = 1$ for all target elements. Here, we reevaluate the model calculations on the basis of the revised ^3He_d and ^{3}H production rates and the measured $P(^3H)/P(^3He)_d$ for most target elements (Table 6). It is important to remember that, for the main target element in stone meteorites (oxygen), there are still no directly measured cross sections; we must derive its contribution by combining complex-target data with single-element target data, which inadvertently results in fairly large uncertainties. Moreover, some of the proton cross sections used for modeling are possibly too low by up to a factor of 2. This would make the inferred neutron excitation functions too high. However, the relative contributions of protons and neutrons to the total ^{3}He production are very similar in the 1.6 GeV target experiments and in meteorites (Leya 1997; Leya et al. 2000b). Therefore, even though the proton-induced fraction may have been underestimated, and the neutron-induced fraction overestimated accordingly, this error would affect the simulation experiments and meteorites to a comparable extent. Since we demonstrated in Figs. 6 and 7 the ability of the model to predict total (i.e., proton + neutron) ^3He_d production rates for the simulation experiments to within a few percent, a similar quality is expected for the total ^{3}He production rates for meteorites.

In Fig. 10, we present modeled $^3He_{cum}/^{21}Ne$ as a function of $^{22}Ne/^{21}Ne$ for H chondrites with radii from 5 cm to 120 cm. As a primary proton spectrum, we used the one given by Castagnoli and Lal (1980), assuming that the modulation parameter of the undisturbed local interstellar cosmic ray spectrum ($\Theta = 0$) is $\Theta = 650$ MeV. This particular choice for the modulation parameter results from fitting the modeled ^{21}Ne production rates to those measured for Knyahinya—an L chondrite with an inferred pre-atmospheric radius of 45 cm (Graf et al. 1990a). For comparison, we show the empirical correlation line for chondrites as given by Nishiizumi et al. (1980), which only differs slightly from the original by Eberhardt et al. (1966). Considering the demands on the model,

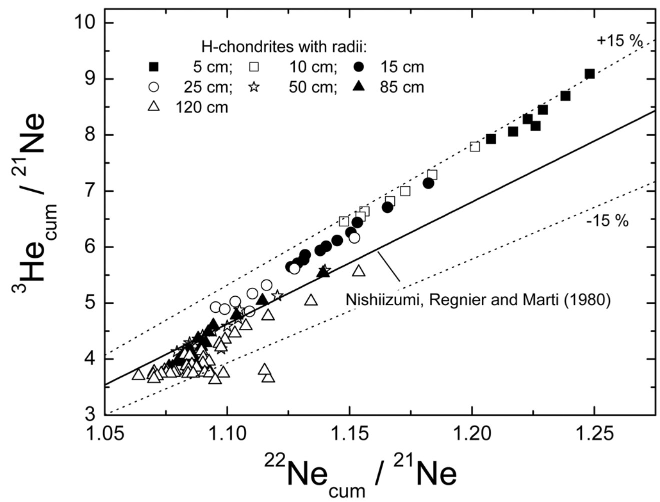

Fig. 10. Modeled $^3He_{cum}/^{21}Ne$ versus $^{22}Ne/^{21}Ne$ for H chondrites with radii between 5 cm and 120 cm. The surface points always plot to the upper right. The center points fall to the lower left except for large radii where $^{22}Ne_{cum}/^{21}Ne$ ratios reach a minimum at a depth of ~150 g × cm^{-2} and then increase again with increasing depth. The solid line represents the empirical correlation given by Nishiizumi et al. (1980). Most calculated data points plot within ±15% in $^3He/^{21}Ne$ ratios of this correlation line. However, we argue that an underestimate, by ~2%, of the calculated $^{22}Ne/^{21}Ne$ ratios for small meteoroids, and low shielding in larger ones, is the more likely reason for the observed discrepancies.

we find the agreement remarkably good. Still, obviously, it is not yet perfect. There is a systematic difference for meteoroids with radii of 15 cm or less and for samples from larger meteoroids shielded by less than ~50 g/cm^2 ($^{22}Ne/^{21}Ne > 1.10$).

A trivial explanation for this offset would be that all small meteoroids, as well as the surface layers of large ones, have suffered diffusive losses of ^{3}H and/or ^{3}He. However, there is ample evidence that this is not a viable explanation. For example, there are numerous small chondrites where ^{3}He cosmic ray exposure ages agree with those based on ^{21}Ne or ^{38}Ar, which are both less prone to be affected by diffusion losses than ^{3}He. Apparently, the reason for the disagreement lies with the model calculations—either the production of ^{3}He is overestimated, or, for small meteorites and little shielding, the calculated $^{22}Ne/^{21}Ne$ ratios come out too small by ~2%. A possible indication that the modeled $^{22}Ne/^{21}Ne$ ratios might be too small is that, for radii of 50 cm or less, the $^3He/^{21}Ne$ versus $^{22}Ne/^{21}Ne$ correlation for samples from within a given-size meteoroid is calculated to be very much the same as it is for all samples so that all data points are aligned along the single correlation line (Fig. 10). However, for meteorites, with one notable exception, the *internal* correlation lines for samples from individual meteorites all tend to be less steep than the mean correlation line in the Berne plot (Wright et al. 1973; Schultz and Signer 1976; Sarafin et al. 1985; Garrison et al. 1992). If, for a given range in $^3He/^{21}Ne$, the model were to yield too small a range in $^{22}Ne/^{21}Ne$, the effect would be as observed. The notable exception where the internal correlation line has the same slope as the general one in the

Berne plot is Knyahinya (for example, see Fig. 4 in Graf et al. [1990b]). At present, it is not clear how much the choice of this atypical (in this respect) meteorite for the adjustment of the model calculations might be the reason for the observed deviation in the slope of the Berne plot correlation line.

Figure 11 shows the depth- and size-dependence of the $^{3}He_{cum}$ production rates for H chondrites with radii from 5 cm up to 120 cm. The modelling is based on the same spectra for primary and secondary particles as those used by Leya et al. (2000a), i.e., a solar modulation parameter Θ = 650 MeV and an integral number of primary GCR particles of 4.06 cm^{-2} sec^{-1}. Primary galactic α particles are taken into account by scaling the production rates due to protons by a factor of 1.55. (For further discussion of α-scaling, see Leya et al. [2000a].)

In Table A1, we present the elemental production rates for the cumulative ^{3}He, i.e. $^{3}He_{d}$ + ^{3}H, from the major target elements. For calculating the cumulative ^{3}He yields, the production rate ratios $P(^{3}H)/P(^{3}He_{d})$ of 0.73, 1.22, 1.28, 1.16, 2.0, and 2.0 for O, Mg, Al, Si, Fe, and Ni, respectively, were used. Although, the data, strictly speaking, are for stony meteorites, we do not anticipate major problems in applying them to other bulk chemical compositions as well because, for the production of ^{3}He and ^{3}H, any matrix effects will only be minor. We used these data to calculate the production rates in ordinary chondrites shown in Figs. 10 and 11. Note that for any given chemical composition within stony meteorites, the production rates can be calculated by the reader. For this purpose, Table A1 is available as an Excel file from the corresponding author.

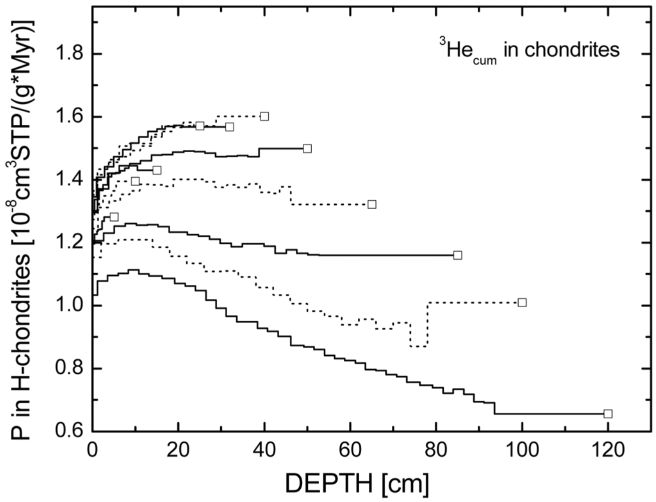

Fig. 11. GCR production rates of $^{3}He_{cum}$ in H chondrites with radii between 5 cm and 120 cm. The model calculations are for a GCR spectrum with a solar modulation parameter Θ = 650 MeV and $J_{0,GCR}$ = 4.06 cm^{-2} s^{-1} as deduced by Leya et al. (2000a). For L chondrites, the numbers have to be multiplied by 1.04. Note that the high production rate at the center of the 100 cm object is due to a computational artifact and has no physical meaning.

CONCLUSIONS

Results from the nuclide production model of Michel et al. (1991, 1996), Leya (1997), and Leya et al. (2000b) agree with the measured noble gas production rates for both 1.6 GeV experiments and three earlier isotropic irradiations of artificial stony meteorites with 600 MeV protons to within ~12%. The new data also demonstrate that the influence on the production rates of the artificial meteoroid's bulk chemical composition (the so called matrix effect) is well-described by the model calculations. This matrix effect is found to be only minor; it shows up most clearly in the production ratios of the Ne isotopes from target elements like Mg, Al, and Si. The agreement between the results of the model calculations and the measured data suggests that the model makes possible a fairly accurate prediction of cosmogenic nuclide production in meteorites and lunar surface material, as well as in terrestrial rocks and the Earth's atmosphere.

Saturation production rates of ^{21}Ne from target elements most relevant in stone meteorites follow the expected spallation systematics; they do suggest, however, that the relative production rate of ^{21}Ne from Si is some 40% lower than commonly assumed, an observation confirmed by recent model calculations for stony meteorites (Leya et al. 2000a)

Targets of metallic Mg and Fe lose their tritium (^{3}H) at a fast rate, but Al and Si, as well as degassed Jilin, apparently do not. Production rate ratios $P(^{3}H)/P(^{3}He)_{d}$ for O, Al, and Si are 0.73, 1.28, and 1.16, respectively. Using these new data, together with the production rates of $^{3}He_{d}$ and ^{21}Ne, model calculations predict, for an H chondrite exposed to the cosmic radiation, a $^{3}He/^{21}Ne$ versus $^{22}Ne/^{21}Ne$ correlation in fair agreement with the empirical Berne plot. The steeper slope of the calculated correlation line is likely due to underestimating, for low shielding, the $^{22}Ne/^{21}Ne$ ratios. Ratios higher by only about 2(!)% would result in perfect agreement.

Acknowledgments–The experiments described here were part of a joint effort of seven European laboratories in Bordeaux, Hannover, Jülich, Köln, Mainz, Paris, and Zürich. The authors are grateful to Drs. U. Herpers, T. Schiekel, F. Sudbrock, and B. Meltzow (Abteilung Nuklearchemie der Universität zu Köln) for their assistance during the irradiations. The technical expertise of Drs. H. Baur and H. Busemann (ETH, Zürich) for the noble gas measurements is appreciated. This work was supported by the Deutsche Forschungsgemeinschaft and the Swiss National Science Foundation. Financial assistance from the Max-Planck-Gesellschaft for irradiation costs is also gratefully acknowledged. The Si material was provided courtesy of Wacker Chemitronic, Burghausen. This work would not have been possible without the skills and assistance of staff members at the Laboratoire National Saturne in Saclay. Reviews by J. Sisterson and M. Honda are appreciated.

Editorial Handling—Dr. Marc Caffee

REFERENCES

Albrecht A., Schnabel C., Vogt S., Xue S., Herzog G. F., Begemann F., Weber H. W., Middleton R., Fink D., and Klein J. 2000. Light noble gases and cosmogenic radionuclides in Estherville, Budulan, and other mesosiderites: Implications for exposure histories and production rates. *Meteoritics & Planetary Science* 35:975–986.

Bainbridge A. E., Suess H. E., and Wänke H. 1962. The tritium content of three stony meteorites and one iron meteorite. *Geochimica et Cosmochimica Acta* 26:471–474.

Begemann F. and Schultz L. 1988. The influence of bulk composition on the production rate of cosmogenic nuclides in meteorites (abstract). 19th Lunar and Planetary Science Conference. pp. 51–52.

Begemann F., Weber H. W., Vilcsek E., and Hintenberger H. 1976. Rare gases and ^{36}Cl in stony meteorites, cosmogenic elemental production rates, exposure ages, diffusion losses, and thermal histories. *Geochimica et Cosmochimica Acta* 40:353–368.

Begemann F., Zhaohui L., Schmitt-Strecker S., Weber H. W., and Zitu X. 1985. Jilin consortium study I: Noble gases and the history of Jilin meteorite. *Earth and Planetary Science Letters* 72:247–262.

Begemann F., Fan C., Weber H. W., and Wang X. 1996. Jilin consortium study II: Light noble gases in Jilin: More of the same and something new. *Meteoritics* 31:667–674.

Castagnoli G. and Lal D. 1980. Solar modulation effects in terrestrial production of carbon-14. *Radiocarbon* 22:133–158.

Dragovitsch P. 1987. Über die Produktion kosmogener Nuklide in Meteoroiden, Simulationsexperimente und Modellrechnungen. Ph.D. thesis, University of Cologne, Köln, Germany.

Dubost H. and Lefort M. 1963. Diffusion of tritium out of iron samples in relation to tritium content in meteorites. *Nature* 200: 566.

Eberhardt P., Eugster O., Geiss J., and Marti K. 1966. Rare gas measurements in 30 stone meteorites. *Zeitschrift Naturforschung Teil A* 21:414–426.

Eugster O. 1988. Cosmic ray production rates of ^{3}He, ^{21}Ne, ^{38}Ar, ^{83}Kr, and ^{126}Xe in chondrites based on ^{81}Kr-Kr exposure ages. *Geochimica et Cosmochimica Acta* 52:1649–1662.

Eugster O. and Michel T. 1995. Common asteroid break-up events of eucrites, diogenites, and howardites and cosmic ray production rates for noble gases in achondrites. *Geochimica et Cosmochimica Acta* 59:177–199.

Fechtig H., Festag J. G., and Schultes H. 1967. Tritium-Diffusionsmessungen an protonenbestrahlten Proben des Eisenmeteoriten Sikhote-Alin. *Zeitschrift Naturforschung Teil A* 22:765–772.

Fireman E. L. and DeFelice J. 1960. Argon-39 and tritium in meteorites. *Geochimica et Cosmochimica Acta* 18:183–192.

Fisher D. E. 1967. Cosmogenic tritium problem in iron meteorites. *Journal of Geophysical Research* 72:1351–1354.

Garrison D. H., Bogard D. D., Albrecht A. A., Vogt S., Herzog G. F., Klein J., Fink D., Dezfouly-Arjomandy B., and Middleton R. 1992. Cosmogenic nuclides in core samples of the Chico L6 chondrite: Evidence for irradiation under high shielding. *Meteoritics* 27:371–381.

Geiss J., Oeschger H., and Schwarz U. 1962. The history of cosmic radiation as revealed by isotopic changes in the meteorites and on the Earth. *Space Science Reviews* 1:197–223.

Graf T., Signer P., Wieler R., Herpers U., Sarafin R., Vogt S., Fieni C., Pellas P., Bonani G., Suter M., and Wölfli W. 1990a. Cosmogenic nuclides and nuclear tracks in the chondrite Knyahinya. *Geochimica et Cosmochimica Acta* 54: 2511–2520.

Graf T., Baur H., and Signer P. 1990b. A model for the production of cosmogenic nuclides in chondrites. *Geochimica et Cosmochimica Acta* 54:2521–2534.

Hintenberger H. and Wänke H. 1964. Helium- und Neonisotope in Eisenmeteoriten. *Zeitschrift Naturforschung Teil A* 19:210–218.

Hintenberger H., Schultz L., Wänke H., and Weber H. 1967. Helium- und Neonisotope in Eisenmeteoriten und der Tritiumverlust in Hexaedriten. *Zeitschrift Naturforschung Teil A* 22:780–787.

Honda M., Caffee M. W., Miura Y. N., Nagai H., Nagao K., and Nishiizumi K. 2002. Cosmogenic nuclides in the Brenham pallasite. *Meteoritics & Planetary Science* 37:1711–1728.

Kirsten T. A. and Schaeffer O. A. 1971. High energy interactions in space. In *Elementary particles,* edited by Yuan L. C. L. New York: Academic Press. pp. 76–157.

Kirsten T, Krankowsky D., and Zähringer J. 1963. Edelgas- und Kalium-Bestimmungen an einer grösseren Zahl von Steinmeteoriten. *Geochimica et Cosmochimica Acta* 27:13–42.

Leya I. 1997. Modellrechnungen zur Beschreibung der Wechselwirkungen galaktischer kosmischer Teilchenstrahlung mit Stein- und Eisenmeteoroiden, Dünntargetbestrahlungen und Dicktargetexperimente. Ph.D. thesis, University of Hannover, Hannover, Germany.

Leya I. and Michel R. 1997. Determination of neutron cross sections for nuclide production at intermediate energies by deconvolution of thick-target production rates. In *Nuclear data for science and technology,* edited by G. Reffo, A. Ventura, and C. Grandi. Bologna: Società di Fisika. pp. 1463–1467.

Leya I., Lange H. J., Neumann S., Wieler R., and Michel R. 2000a. The production of cosmogenic nuclides in stony meteoroids by galactic cosmic ray particles. *Meteoritics & Planetary Science* 35:259–286.

Leya I., Lange H. J., Lüpke M., Neupert U., Daunke R., Fanenbruck O., Michel R., Rösel R., Meltzow B., Schiekel T., Sudbrock F., Herpers U., Filges D., Bonani G., Dittrich-Hannen B., Suter M., Kubik P. W., and Synal H. A. 2000b. Simulation of the interaction of galactic cosmic-ray protons with meteoroids: On the production of radionuclides in thick gabbro and iron targets irradiated isotropically with 1.6 GeV protons. *Meteoritics & Planetary Science* 35:287–318.

Leya I., Neumann S., Wieler R., and Michel R. 2001. The production of cosmogenic nuclides by galactic cosmic ray particles for 2π exposure geometries. *Meteoritics & Planetary Science* 36:1547–1561.

Lüpke M. 1993. Untersuchungen zur Wechselwirkungen galaktischer Protonen mit Meteoroiden- Dicktarget- Simulationsexperimente und Messung von Dünntarget-Wirkungsquerschnitten. Ph.D. thesis, University of Hannover, Hannover, Germany.

Masarik J. and Reedy R.C. 1994. Effects of bulk composition on nuclide production processes in meteorites. *Geochimica et Cosmochimica Acta* 58:5307–5317.

Mason B. 1971. *Handbook of elemental abundances in meteorites.* New York: Gordon and Breach.

Michel R., Dragovitsch P., Englert P., Peiffer F., Stück R., Theis S., Begemann F., Weber H., Signer P., Wieler R., Filges D., and Cloth P. 1986. On the depth dependence of spallation reactions in a spherical thick diorite target homogeneously irradiated by 600 MeV protons. Simulation of production of cosmogenic nuclides in small meteorites. *Nuclear Instruments and Methods in Physics Research B* 16:61–82.

Michel R., Peiffer F., Theis S., Begemann F., Weber H., Signer P., Wieler R., Cloth P., Dragovitsch P., Filges D., and Englert P. 1989. Production of stable and radioactive nuclides in thick stony targets (R = 15 and 25 cm) isotropically irradiated with 600 MeV protons and simulation of the production of cosmogenic nuclides in meteorites. *Nuclear Instruments and Methods in Physics Research B* 42:76–100.

Michel R., Dragovitsch P., Cloth P., Dagge G., and Filges D. 1991. On the production of cosmogenic nuclides in meteoroids by galactic protons. *Meteoritics* 26:221–242.

Michel R., Leya I., and Borges L. 1996. Production of cosmogenic nuclides in meteoroids: Accelerator experiments and model calculations to decipher the cosmic ray record in extraterrestrial matter. *Nuclear Instruments and Methods in Physics Research B* 113:434–444.

Nishiizumi K., Regnier S., and Marti K. 1980. Cosmic ray exposure ages, pre-irradiation, and constancy of cosmic ray flux in the past. *Earth and Planetary Science Letters* 50:156–170.

Nyquist L., Funk H., Schultz L., and Signer P. 1973. He, Ne, and Ar in chondritic Ni-Fe as irradiation hardness sensors. *Geochimica et Cosmochimica Acta* 37:1655–1685.

Sarafin R., Bourot-Denise M., Crosaz G., Herpers U., Pellas P., Schultz L., and Weber H.W. 1985. Cosmic ray effects in the Antarctic meteorite Allan Hills A 78084. *Earth and Planetary Science Letters* 73:171–183.

Schultz L. and Signer P. 1976. Depth dependence of spallogenic helium, neon, and argon in the St. Severin chondrite. *Earth and Planetary Science Letters* 30:191–199.

Schultz L. and Freundel M. 1985. On the production rate of ^{21}Ne in ordinary chondrites. In *Isotopic ratios in the solar system,* edited by Centre National d'Etudes Spatiales. Paris: Cepadues-Editions. pp. 27–33.

Smith S.P. and Huneke J.C. 1975. Cosmogenic neon produced from sodium in meteoritic minerals. *Earth and Planetary Science Letters* 27:191–199.

von Michaelis H., Ahrens L. H., and Willis J. P. 1969. The composition of stony meteorites II: The analytical data and an assessment of their quality. *Earth and Planetary Science Letters* 5:387–394.

Voshage H. and Feldmann H. 1979. Investigations on cosmic ray-produced nuclides in iron meteorites: 3. Exposure ages, meteoroid sizes, and sample depths determined by mass spectrometric analyses of potassium and rare gases. *Earth and Planetary Science Letters* 45:293–308.

Wright R. J., Simms L. A., Reynolds M. A., and Bogard D. D. 1973. Depth variation of cosmogenic noble gases in the ~120 kg Keyes chondrite. *Journal of Geophysical Research* 78:1308–1318.

Zähringer J. 1966. Die Chronologie der Chondriten aufgrund von Edelgasisotopen-Analysen. *Meteoritika* 27:25–40. In Russian.

APPENDIX

Table A1. Calculated elemental GCR production rates for the cumulative production of ^3He_c as a function of radius (R) and shielding depth (d/R) inside stony meteoroids.[a]

Elemental production rates (10^{-8} cm^3 STP/g/Myr)

Radius (cm)	Depth d/R	^3He_c from O	Mg	Al	Si	Fe	Ni	Radius (cm)	Depth d/R	^3He_c from O	Mg	Al	Si	Fe	Ni
5	0.00–0.10	1.265	1.172	1.270	1.385	1.209	1.485		0.50–0.60	2.205	1.847	1.370	1.525	1.209	1.473
	0.10–0.20	1.328	1.208	1.290	1.413	1.218	1.497		0.60–0.70	2.260	1.894	1.388	1.553	1.218	1.485
	0.20–0.30	1.357	1.234	1.290	1.413	1.218	1.497		0.70–1.00	2.332	1.938	1.405	1.570	1.230	1.497
	0.30–0.40	1.378	1.243	1.290	1.413	1.218	1.497	32	0.00–0.06	1.766	1.523	1.281	1.430	1.173	1.437
	0.40–0.50	1.385	1.252	1.290	1.413	1.215	1.485		0.06–0.12	1.935	1.641	1.308	1.464	1.182	1.437
	0.50–0.60	1.427	1.281	1.316	1.439	1.230	1.509		0.12–0.19	2.034	1.712	1.325	1.482	1.185	1.449
	0.60–1.00	1.448	1.308	1.325	1.447	1.242	1.521		0.19–0.25	2.119	1.776	1.334	1.499	1.185	1.437
10	0.00–0.10	1.441	1.308	1.316	1.439	1.230	1.509		0.25–0.31	2.184	1.820	1.343	1.508	1.185	1.449
	0.10–0.20	1.526	1.361	1.325	1.456	1.230	1.509		0.31–0.37	2.246	1.865	1.352	1.516	1.188	1.449
	0.20–0.30	1.590	1.405	1.334	1.464	1.242	1.509		0.37–0.44	2.295	1.903	1.352	1.525	1.188	1.449
	0.30–0.40	1.639	1.443	1.352	1.482	1.242	1.521		0.44–0.50	2.339	1.938	1.370	1.544	1.197	1.449
	0.40–0.50	1.660	1.452	1.352	1.473	1.242	1.509		0.50–0.56	2.366	1.956	1.370	1.544	1.200	1.449
	0.50–0.60	1.688	1.479	1.361	1.490	1.242	1.521		0.56–0.62	2.394	1.974	1.370	1.544	1.191	1.449
	0.60–1.00	1.745	1.523	1.388	1.516	1.266	1.548		0.62–0.69	2.408	1.982	1.352	1.544	1.182	1.437
15	0.00–0.07	1.540	1.370	1.308	1.439	1.218	1.485		0.69–0.75	2.424	1.982	1.343	1.536	1.176	1.425
	0.07–0.13	1.646	1.443	1.325	1.464	1.230	1.497		0.75–1.00	2.401	2.000	1.370	1.536	1.182	1.437
	0.13–0.20	1.717	1.487	1.343	1.482	1.230	1.509	40	0.00–0.06	1.822	1.558	1.261	1.421	1.155	1.413
	0.20–0.27	1.766	1.532	1.352	1.490	1.242	1.509		0.06–0.12	1.999	1.685	1.290	1.456	1.158	1.413
	0.27–0.33	1.815	1.567	1.379	1.508	1.254	1.521		0.12–0.19	2.119	1.767	1.299	1.473	1.158	1.413
	0.33–0.40	1.851	1.596	1.379	1.516	1.242	1.521		0.19–0.25	2.191	1.820	1.299	1.473	1.146	1.401
	0.40–0.47	1.865	1.605	1.370	1.508	1.242	1.509		0.25–0.31	2.253	1.865	1.308	1.482	1.146	1.389
	0.47–0.53	1.886	1.614	1.379	1.516	1.242	1.509		0.31–0.37	2.304	1.903	1.308	1.482	1.146	1.389
	0.53–0.60	1.914	1.632	1.379	1.516	1.242	1.509		0.37–0.44	2.373	1.956	1.316	1.499	1.149	1.401
	0.60–0.67	1.928	1.649	1.379	1.525	1.242	1.509		0.44–0.50	2.424	1.991	1.325	1.508	1.152	1.401
	0.67–0.73	1.944	1.658	1.379	1.516	1.242	1.509		0.50–0.56	2.466	2.018	1.325	1.516	1.152	1.401
	0.73–1.00	1.928	1.641	1.352	1.499	1.218	1.485		0.56–0.62	2.500	2.056	1.343	1.525	1.158	1.413
25	0.00–0.10	1.759	1.523	1.325	1.464	1.212	1.485		0.62–0.69	2.480	2.038	1.325	1.516	1.146	1.389
	0.10–0.20	1.944	1.658	1.352	1.499	1.218	1.485		0.69–0.75	2.500	2.047	1.308	1.508	1.137	1.377
	0.20–0.30	2.041	1.732	1.361	1.508	1.215	1.485		0.75–1.00	2.565	2.100	1.334	1.536	1.155	1.401
	0.30–0.40	2.140	1.803	1.388	1.544	1.230	1.497	50	0.00–0.05	1.773	1.505	1.190	1.350	1.089	1.329
	0.40–0.50	2.191	1.829	1.379	1.536	1.218	1.485		0.05–0.10	1.978	1.641	1.225	1.395	1.098	1.341

Table A1. Calculated elemental GCR production rates for the cumulative production of $^{3}He_{c}$ as a function of radius (R) and shielding depth (d/R) inside stony meteoroids.[a] *Continued.*

Elemental production rates (10^{-8} cm^{3} STP/g/Myr)															
Radius	Depth	$^{3}He_{c}$ from						Radius	Depth	$^{3}He_{c}$ from					
(cm)	d/R	O	Mg	Al	Si	Fe	Ni	(cm)	d/R	O	Mg	Al	Si	Fe	Ni
50	0.10–0.15	2.112	1.740	1.243	1.421	1.107	1.353		0.04–0.08	1.787	1.479	1.037	1.192	0.921	1.128
	0.15–0.20	2.184	1.803	1.252	1.430	1.107	1.353		0.08–0.12	1.879	1.541	1.019	1.184	0.894	1.092
	0.20–0.25	2.239	1.829	1.234	1.421	1.089	1.329		0.12–0.16	1.921	1.567	1.001	1.166	0.873	1.065
	0.25–0.30	2.274	1.865	1.234	1.421	1.080	1.314		0.16–0.20	1.928	1.558	0.963	1.132	0.837	1.020
	0.30–0.35	2.325	1.903	1.234	1.430	1.080	1.314		0.20–0.24	1.900	1.541	0.928	1.095	0.801	0.975
	0.35–0.40	2.352	1.920	1.234	1.421	1.071	1.302		0.24–0.28	1.886	1.523	0.892	1.061	0.771	0.939
	0.40–0.45	2.387	1.938	1.225	1.421	1.062	1.290		0.28–0.32	1.879	1.505	0.859	1.026	0.738	0.900
	0.45–0.50	2.417	1.956	1.240	1.413	1.050	1.278		0.32–0.36	1.907	1.523	0.844	1.017	0.729	0.888
	0.50–0.55	2.417	1.965	1.249	1.421	1.050	1.278		0.36–0.40	1.893	1.496	0.813	0.991	0.705	0.858
	0.55–0.60	2.424	1.965	1.231	1.404	1.038	1.266		0.40–0.44	1.837	1.452	0.784	0.966	0.678	0.828
	0.60–0.65	2.417	1.965	1.222	1.395	1.026	1.242		0.44–0.48	1.808	1.434	0.759	0.937	0.654	0.801
	0.65–0.70	2.438	1.956	1.204	1.385	1.014	1.230		0.48–0.52	1.766	1.396	0.733	0.912	0.630	0.771
	0.70–0.75	2.438	1.965	1.213	1.395	1.023	1.242		0.52–0.56	1.738	1.370	0.713	0.886	0.612	0.750
	0.75–0.80	2.431	1.965	1.222	1.385	1.026	1.242		0.56–0.60	1.717	1.352	0.693	0.866	0.597	0.735
	0.80–1.00	2.452	2.000	1.259	1.421	1.053	1.278		0.60–0.64	1.695	1.316	0.646	0.832	0.564	0.693
65	0.00–0.04	1.710	1.452	1.167	1.298	1.041	1.266		0.64–0.68	1.731	1.334	0.657	0.845	0.573	0.705
	0.04–0.08	1.900	1.587	1.204	1.333	1.050	1.278		0.68–0.72	1.681	1.299	0.642	0.819	0.555	0.684
	0.08–0.12	1.985	1.649	1.195	1.333	1.035	1.266		0.72–0.76	1.710	1.325	0.662	0.836	0.570	0.699
	0.12–0.15	2.071	1.694	1.186	1.333	1.023	1.254		0.76–0.80	1.597	1.225	0.579	0.760	0.507	0.624
	0.15–0.19	2.119	1.740	1.186	1.333	1.011	1.230		0.80–1.00	1.590	1.261	0.622	0.791	0.537	0.657
	0.19–0.23	2.184	1.785	1.186	1.341	1.011	1.230	120	0.00–0.02	1.420	1.217	0.963	1.106	0.888	1.086
	0.23–0.27	2.212	1.794	1.167	1.324	0.990	1.209		0.02–0.04	1.575	1.316	0.963	1.115	0.867	1.062
	0.27–0.31	2.232	1.803	1.147	1.315	0.975	1.191		0.04–0.06	1.653	1.361	0.955	1.106	0.849	1.035
	0.31–0.35	2.288	1.847	1.156	1.324	0.981	1.194		0.06–0.08	1.710	1.396	0.937	1.095	0.834	1.017
	0.35–0.38	2.304	1.865	1.156	1.324	0.978	1.188		0.08–0.10	1.752	1.434	0.928	1.086	0.819	0.999
	0.38–0.42	2.318	1.874	1.147	1.315	0.966	1.176		0.10–0.12	1.759	1.434	0.919	1.069	0.801	0.975
	0.42–0.46	2.318	1.865	1.129	1.307	0.951	1.161		0.12–0.15	1.773	1.434	0.892	1.052	0.777	0.945
	0.46–0.50	2.304	1.847	1.110	1.281	0.933	1.137		0.15–0.17	1.794	1.443	0.870	1.035	0.759	0.927
	0.50–0.54	2.332	1.865	1.101	1.281	0.930	1.134		0.17–0.19	1.773	1.434	0.855	1.009	0.741	0.903
	0.54–0.58	2.318	1.865	1.101	1.272	0.924	1.128		0.19–0.21	1.780	1.434	0.835	1.000	0.720	0.879
	0.58–0.62	2.346	1.894	1.110	1.281	0.927	1.131		0.21–0.23	1.766	1.423	0.821	0.983	0.708	0.864
	0.62–0.65	2.318	1.856	1.083	1.255	0.900	1.101		0.23–0.25	1.731	1.379	0.788	0.946	0.681	0.834
	0.65–0.69	2.325	1.847	1.065	1.246	0.888	1.086		0.25–0.27	1.702	1.361	0.761	0.920	0.657	0.804
	0.69–0.73	2.359	1.885	1.092	1.264	0.909	1.107		0.27–0.29	1.681	1.325	0.722	0.886	0.627	0.765
	0.73–1.00	2.274	1.794	1.028	1.201	0.861	1.050		0.29–0.31	1.646	1.308	0.706	0.866	0.609	0.744
85	0.00–0.03	1.597	1.352	1.063	1.210	0.972	1.188		0.31–0.33	1.653	1.316	0.710	0.866	0.609	0.747
	0.03–0.06	1.745	1.461	1.081	1.227	0.969	1.182		0.33–0.35	1.618	1.290	0.688	0.845	0.591	0.723
	0.06–0.09	1.837	1.523	1.072	1.227	0.954	1.164		0.35–0.37	1.618	1.281	0.670	0.832	0.579	0.711
	0.09–0.12	1.921	1.578	1.072	1.236	0.945	1.152		0.37–0.40	1.604	1.252	0.650	0.814	0.564	0.693
	0.12–0.15	1.971	1.614	1.055	1.227	0.930	1.134		0.40–0.42	1.554	1.208	0.624	0.784	0.543	0.669
	0.15–0.18	1.999	1.623	1.037	1.210	0.909	1.107		0.42–0.44	1.547	1.208	0.619	0.780	0.537	0.657
	0.18–0.21	2.027	1.649	1.028	1.201	0.894	1.092		0.44–0.46	1.540	1.208	0.622	0.773	0.537	0.654
	0.21–0.24	2.048	1.649	1.010	1.184	0.876	1.068		0.46–0.48	1.505	1.190	0.608	0.756	0.522	0.639
	0.24–0.26	2.034	1.641	0.992	1.166	0.855	1.044		0.48–0.50	1.491	1.181	0.597	0.741	0.510	0.624
	0.26–0.29	2.041	1.649	0.983	1.158	0.849	1.035		0.50–0.52	1.477	1.163	0.582	0.730	0.498	0.612
	0.29–0.32	2.048	1.641	0.963	1.149	0.837	1.017		0.52–0.54	1.477	1.154	0.591	0.728	0.498	0.609
	0.32–0.35	2.055	1.641	0.955	1.140	0.825	1.005		0.54–0.56	1.434	1.126	0.579	0.706	0.483	0.591
	0.35–0.38	2.048	1.641	0.946	1.123	0.813	0.990		0.56–0.58	1.427	1.126	0.584	0.706	0.486	0.597
	0.38–0.41	2.041	1.632	0.928	1.106	0.798	0.972		0.58–0.60	1.406	1.108	0.570	0.696	0.474	0.582
	0.41–0.44	2.034	1.623	0.910	1.086	0.780	0.951		0.60–0.62	1.406	1.099	0.565	0.689	0.474	0.582
	0.44–0.47	2.071	1.641	0.910	1.095	0.780	0.951		0.62–0.65	1.378	1.081	0.556	0.672	0.465	0.567
	0.47–0.50	2.071	1.649	0.910	1.095	0.777	0.948		0.65–0.67	1.378	1.063	0.531	0.654	0.450	0.552
	0.50–0.53	2.064	1.649	0.895	1.078	0.765	0.933		0.67–0.69	1.357	1.055	0.522	0.646	0.435	0.534
	0.53–0.56	2.048	1.614	0.864	1.061	0.744	0.906		0.69–0.71	1.307	1.037	0.518	0.635	0.429	0.528
	0.56–0.59	2.055	1.632	0.875	1.069	0.753	0.921		0.71–0.73	1.321	1.055	0.529	0.648	0.438	0.537
	0.59–0.62	2.034	1.614	0.859	1.052	0.741	0.906		0.73–0.75	1.300	1.046	0.543	0.648	0.447	0.546
	0.62–0.65	2.055	1.614	0.833	1.043	0.717	0.876		0.75–0.77	1.279	1.010	0.472	0.607	0.396	0.486
	0.65–1.00	2.041	1.623	0.848	1.043	0.726	0.885		0.77–0.79	1.286	1.001	0.479	0.609	0.402	0.498
100	0.00–0.04	1.618	1.361	1.046	1.192	0.948	1.161		0.79–1.00	1.138	0.888	0.404	0.531	0.336	0.417

[a] The cumulative ^{3}He yields were calculated using production rate ratios $P(^{3}H)/P(^{3}He_{d})$ = 0.73, 1.22, 1.28, 1.16, 2.0, and 2.0 for O, Mg, Al, Si, Fe and Ni, respectively.